AD-A065 043 TECHNOLOGY SERVICE CORP SANTA MONICA CALIF F/G 20/6
DATA BASE DESCRIPTORS FOR ELECTRO-OPTICAL SENSOR SIMULATION.(U)
FEB 79 T A ZIMMERLIN, G J SUTTY, A J STENGER F33615-77-C-0049
UNCLASSIFIED AFHRL-TR-78-86 NL

| OF |
AD
A065043

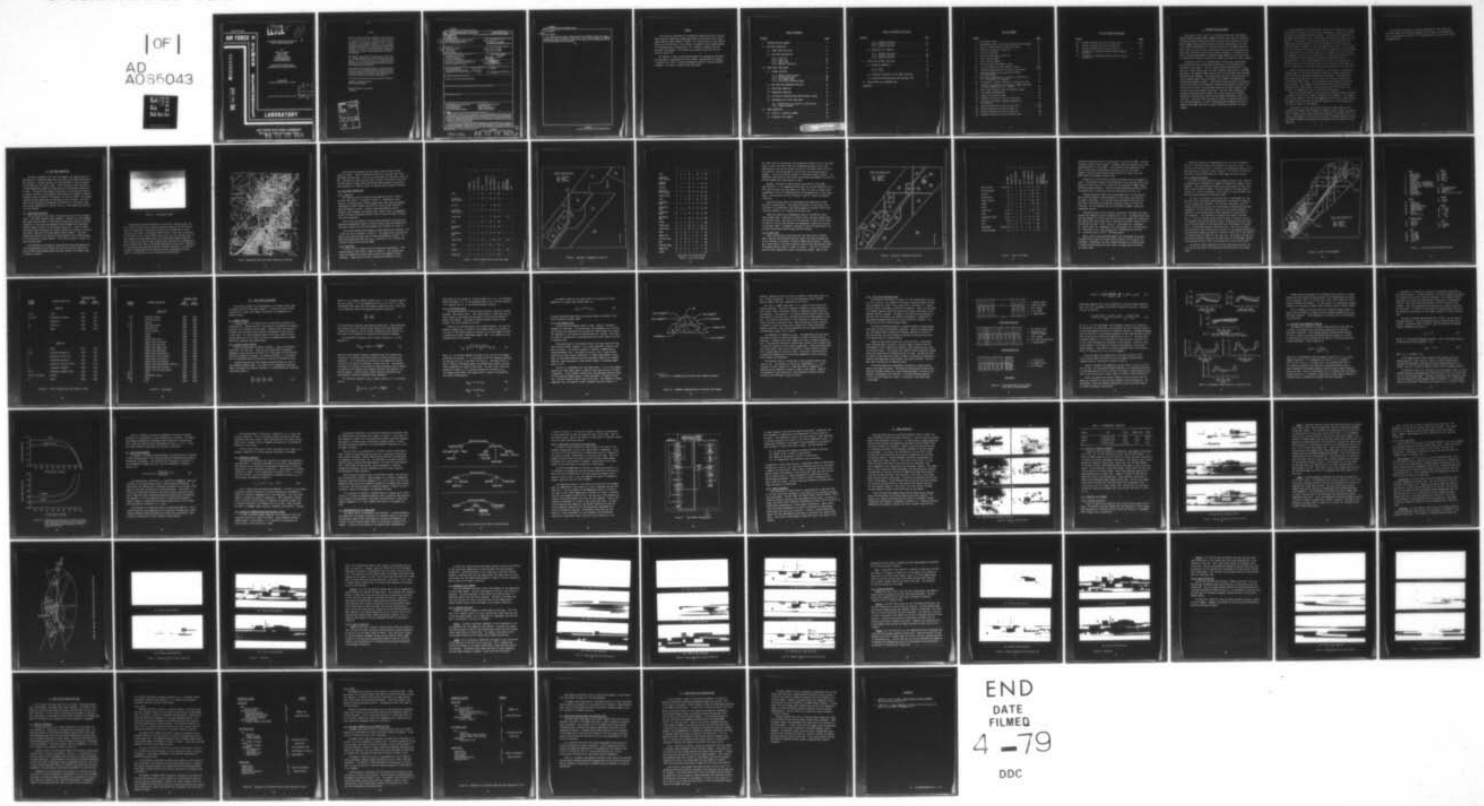

END
DATE
FILMED
4-79
DDC

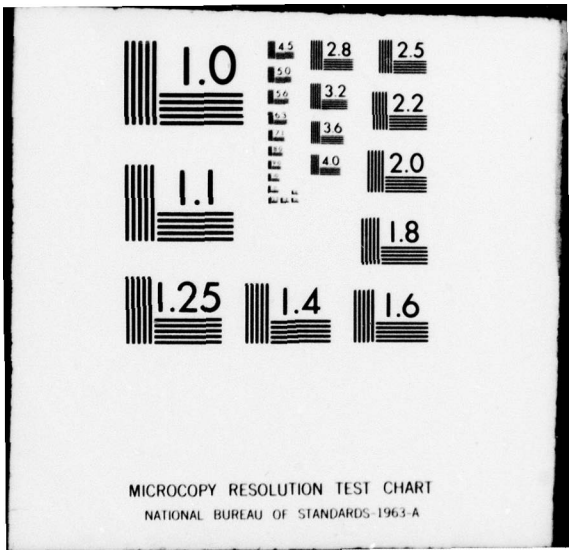
1.0
1.1
1.25
1.4
1.6
1.8
2.0
2.2
2.5
2.8
3.2
3.6
4.0
4.5
5.0
5.6
MICROCOPY RESOLUTION TEST CHART
NATIONAL BUREAU OF STANDARDS-1963-A

AFHRL-TR-78-86

LEVEL II

AIR FORCE HUMAN RESOURCES LABORATORY

AD A065043

DDC FILE COPY

DATA BASE DESCRIPTORS FOR ELECTRO-OPTICAL SENSOR SIMULATION

By

Timothy A. Zimmerlin
George J. Sutty
Anthony J. Stenger

Technology Service Corporation
2811 Wilshire Boulevard
Santa Monica, California 90403

ADVANCED SYSTEMS DIVISION
Wright-Patterson Air Force Base, Ohio 45433

February 1979
Final Report for Period May 1977 – June 1978

Approved for public release; distribution unlimited.

AIR FORCE SYSTEMS COMMAND
BROOKS AIR FORCE BASE, TEXAS 78235

NOTICE

When U.S. Government drawings, specifications, or other data are used for any purpose other than a definitely related Government procurement operation, the Government thereby incurs no responsibility nor any obligation whatsoever, and the fact that the Government may have formulated, furnished, or in any way supplied the said drawings, specifications, or other data is not to be regarded by implication or otherwise, as in any manner licensing the holder or any other person or corporation, or conveying any rights or permission to manufacture, use, or sell any patented invention that may in any way be related thereto.

This final report was prepared by Technology Service Corporation, 2811 Wilshire Boulevard, Santa Monica, California 90403 under contract F33615-77-C-0049, project 6114, with Advanced Systems Division, Air Force Human Resources Laboratory (AFSC), Wright-Patterson Air Force Base, Ohio 45433. Mr. Michael R. Nicol was the Contract Monitor for the Laboratory.

This report has been reviewed and cleared for open publication and/or public release by the appropriate Office of Information (OI) in accordance with AFR 190-17 and DoDD 5230.9. There is no objection to unlimited distribution of this report to the public at large, or by DDC to the National Technical Information Service (NTIS).

This technical report has been reviewed and is approved for publication.

GORDON A. ECKSTRAND, Director
Advanced Systems Division

RONALD W. TERRY, Colonel, USAF
Commander

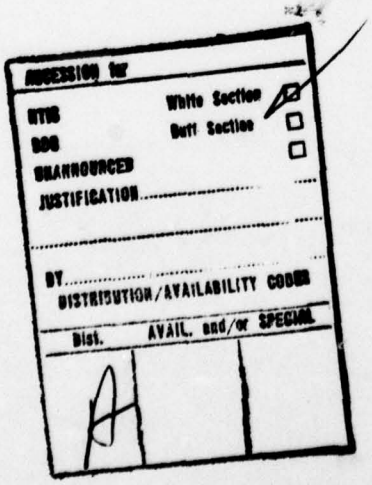

Unclassified

SECURITY CLASSIFICATION OF THIS PAGE *(When Data Entered)*

(18) (19) **REPORT DOCUMENTATION PAGE**

READ INSTRUCTIONS BEFORE COMPLETING FORM

1. REPORT NUMBER: AFHRL-TR-78-86

2. GOVT ACCESSION NO.

3. RECIPIENT'S CATALOG NUMBER

(6) 4. TITLE *(and Subtitle)*: DATA BASE DESCRIPTORS FOR ELECTRO-OPTICAL SENSOR SIMULATION

(9) 5. TYPE OF REPORT & PERIOD COVERED: Final rept. May 1977 – June 1978

6. PERFORMING ORG. REPORT NUMBER

(10) 7. AUTHOR(s): Timothy A. Zimmerlin, George J. Sutty, Anthony J. Stenger

(15) 8. CONTRACT OR GRANT NUMBER(s): F33615-77-C-0049

9. PERFORMING ORGANIZATION NAME AND ADDRESS: Technology Service Corporation, 2811 Wilshire Boulevard, Santa Monica, California 90403

(16) 10. PROGRAM ELEMENT, PROJECT, TASK AREA & WORK UNIT NUMBERS: 62205F, 6114 (17) 14 415

11. CONTROLLING OFFICE NAME AND ADDRESS: HQ Air Force Human Resources Laboratory (AFSC), Brooks Air Force Base, Texas 78235

(11) 12. REPORT DATE: February 1979

13. NUMBER OF PAGES: 76

14. MONITORING AGENCY NAME & ADDRESS *(if different from Controlling Office)*: Advanced Systems Division, Air Force Human Resources Laboratory, Wright-Patterson Air Force Base, Ohio 45433 (12) 77p.

15. SECURITY CLASS. *(of this report)*: Unclassified

15a. DECLASSIFICATION/DOWNGRADING SCHEDULE

16. DISTRIBUTION STATEMENT *(of this Report)*

Approved for public release; distribution unlimited.

17. DISTRIBUTION STATEMENT *(of the abstract entered in Block 20, if different from Report)*

18. SUPPLEMENTARY NOTES

19. KEY WORDS *(Continue on reverse side if necessary and identify by block number)*

Defense Mapping Agency Aerospace Center
digital data base descriptors
electro-optical simulation
Forward Looking Infrared Simulation
Low Light Level Television Simulation
thermal model for IR
imagery from passive sensors
Computer Image Generation

20. ABSTRACT *(Continue on reverse side if necessary and identify by block number)*

The purpose of this study is to investigate the use of the Defense Mapping Agency Aerospace Center (DMAAC) digital source data for simulation of Forward Looking Infrared (FLIR) and Low Light Level Television (LLLTV) sensor imagery during various periods of the day and seasons of the year. This includes determination of deficiencies of the DMAAC data base which limit its use as well as identification of additional parameters which would increase its utility for sensor simulation.

The approach taken in the study was to determine what information is required of the scene, its environment, and the sensor and to generate realistic imagery from it. Then imagery using lesser amounts of data can be generated for various user applications. The impact on the data base can then be assessed for a given application and level of

→ next page

DD FORM 1 JAN 73 1473 EDITION OF 1 NOV 65 IS OBSOLETE

Unclassified

SECURITY CLASSIFICATION OF THIS PAGE *(When Data Entered)*

Item 20 Continued:

detail in the imagery.

The results of this study include a realistic tonal model for the simulation of passive sensor imagery of complex cultural scenes, the generation of imagery from a scene constructed according to the DMAAC specifications, an assessment of the resultant diurnal and seasonal imagery, and the relationship between the model data requirements and the resources of the data base.

PREFACE

This study was performed for the Advanced Systems Division, Air Force Human Resources Laboratory, Wright-Patterson Air Force Base, Ohio, 45433, under contract number F33615-77-C-0049. Mr. Michael Nicol was the contract monitor for the Air Force. Mr. Anthony J. Stenger was the program manager for Technology Service Corporation. Mr. Timothy A. Zimmerlin was the principal investigator. The research was started in May 1977 and completed in June 1978.

Mr. George J. Sutty contributed throughout the program and developed the data bases, implemented the thermal model, and generated the imagery. In addition, Mr. John D. Stanley developed the material and environmental languages. Ms. Dona K. Reynolds typed the report.

TABLE OF CONTENTS

TABLE OF CONTENTS (Continued)

LIST OF FIGURES

LIST OF FIGURES (Continued)

I. INTRODUCTION AND SUMMARY

The purpose of this study is to investigate the use of the Defense Mapping Agency Aerospace Center (DMAAC) digital source data for simulation of Forward Looking Infrared (FLIR) and Low Light Level Television (LLLTV) sensor imagery during various periods of the day and seasons of the year. This includes determination of those deficiencies of the DMAAC data base which limit its use as well as identification of the additional parameters which would increase its utility for sensor simulation. In addition, the effort involves development of Computer Image Generation (CIG) algorithms to simulate the effects of diurnal and seasonal variations on sensor imagery.

In order to fulfill the intended goals of this study, the approach was divided into four tasks which are described in the following four sections of this report. The first task involved construction of a data base for a chosen target area for three different resolutions of the DMAAC data base. The subject target area was one of 16 available from the AFHRL Seasonal Sensor Handbook. The second task consisted of the derivation of fairly sophisticated visual and thermal tonal models from theoretical thermo-electromagnetic models. These models blend the physical properties of the scene with the environmental conditions and particular sensor characteristics to result in an accurate simulation of sensor imagery under various diurnal and seasonal conditions. The third task consisted of generating simulated sensor imagery for various diurnal and seasonal conditions using the data bases and tonal models developed in the first two tasks. The fourth task consisted of analysis of the deficiencies of the simulated imagery, in order to determine what parameters need to be added to the DMAAC data base to support effective simulation of sensor imagery.

At the beginning of the program the intent was to generate the imagery with a modest extension of the data base requirements. However, some shortcomings were associated with this approach. The 12 material codes used in the DMAAC specification do not fully reflect the physical properties of the material. For example, in the scene evaluated in this study, both the cement plant and the hospital have the same material code yet they have different thermal properties. Also, the DMAAC feature code is use oriented and is not related to the reflective or emissive properties of the buildings. Thus, the hospital has a feature code that is identical to that of schools and churches, all of which are identified as institutional structures, but this identification has nothing to do with the underlying physical characteristics. With limited additional descriptors in the data base, it was felt that only a little more fidelity could be added to the simulated passive imagery which is derived through transformations of the DMAAC data.

A basis of much of the tonal modeling is the result of a measurement program under Air Force Human Resources Laboratory (AFHRL) sponsorship, which resulted in the AFHRL Seasonal Sensor Handbook. The measurements were taken on multiple days in each of the four seasons of the year on 16 different target scenes. The instrument and environmental conditions were recorded. This handbook provided a qualitative source during the formation of the tonal models. Also, once the models and imagery were derived, the handbook was used for qualitative evaluation.

Thus, the approach taken in the study was to determine what information is needed to simulate the imagery contained in the handbook. Then imagery using lesser amounts of data can be generated for various user applications. The impact on the data base can then be assessed for a given application and level of detail in the imagery.

The results of this study include a realistic tonal model for the simulation of passive sensor imagery of complex cultural scenes, the generation of imagery from a scene constructed according to the DMAAC specifications, an assessment of the resultant diurnal and seasonal imagery, and the relationship between the model data requirements and the resources of the data base.

The following sections of the report describe the scene data base, the tonal models, the simulated imagery, and the impact on the DMAAC data base. The technical discussion is followed by the conclusions and research recommendations.

II. DATA BASE GENERATION

In order to generate LLLTV and FLIR imagery, the construction of a data base for a selected target area according to the DMAAC specification was required. The data necessary for the simulation of sensor imagery are divided into three basic types. The first type of data consists of a three-dimensional geometrical description of the features contained in a scene. The second type contains descriptions of the physical make-up of typical surfaces in the geometric data base and is needed to simulate different types of sensors; for example, for the FLIR sensor, the thermal conductivity and capacitance of the material must be known. The third type of data describes environmental conditions for a particular scene and includes temperature of the sun, sky, air, wind speed and direction, and precipitation.

2.1 TARGET AREA SELECTION

The first task of this effort involved evaluation of the 16 target areas in the AFHRL Seasonal Sensor Handbook. The data for this handbook were taken from the tower of the Avionics Laboratory building at Wright-Patterson Air Force Base and spanned the area between the flight maintenance hangars of Area C to the Trebein radar dish. Scenes in these recordings range from nearly all natural content to a mixture of cultural and natural features with rather dense cultural content. The scene showing the hospital was chosen to be the subject of this study because of its variety of cultural content. This scene is shown in Figure 1 as seen from the tower.

The selection of the hospital scene required data base modeling of a strip approximately 2-1/2 miles long and 3/4 mile wide, parallel to the railroad tracks between Dayton and Xenia Avenues in Fairborn, Ohio, as shown in Figure 2.

Figure 1. The Hospital Scene

Photographs taken from the tower at the Avionics Laboratory were the major source of data used in selecting important features for the construction of the data base. Since not all details of the scene were visible from that view, some of the features were omitted. Effort was concentrated on the hospital (1), officers family housing (2), the base heating plant (3), the Southwest Portland Cement Plant (4), and the Maple Avenue bridge (5). Exact relative positions of these features were obtained from a geographical map of Fairborn and a map of the Wright-Patterson Air Force Base. Dimensions of the features were extracted from the available blueprints. In addition, a number of photographs of the buildings and the surrounding areas were taken as an interpretative aid in the data base construction.

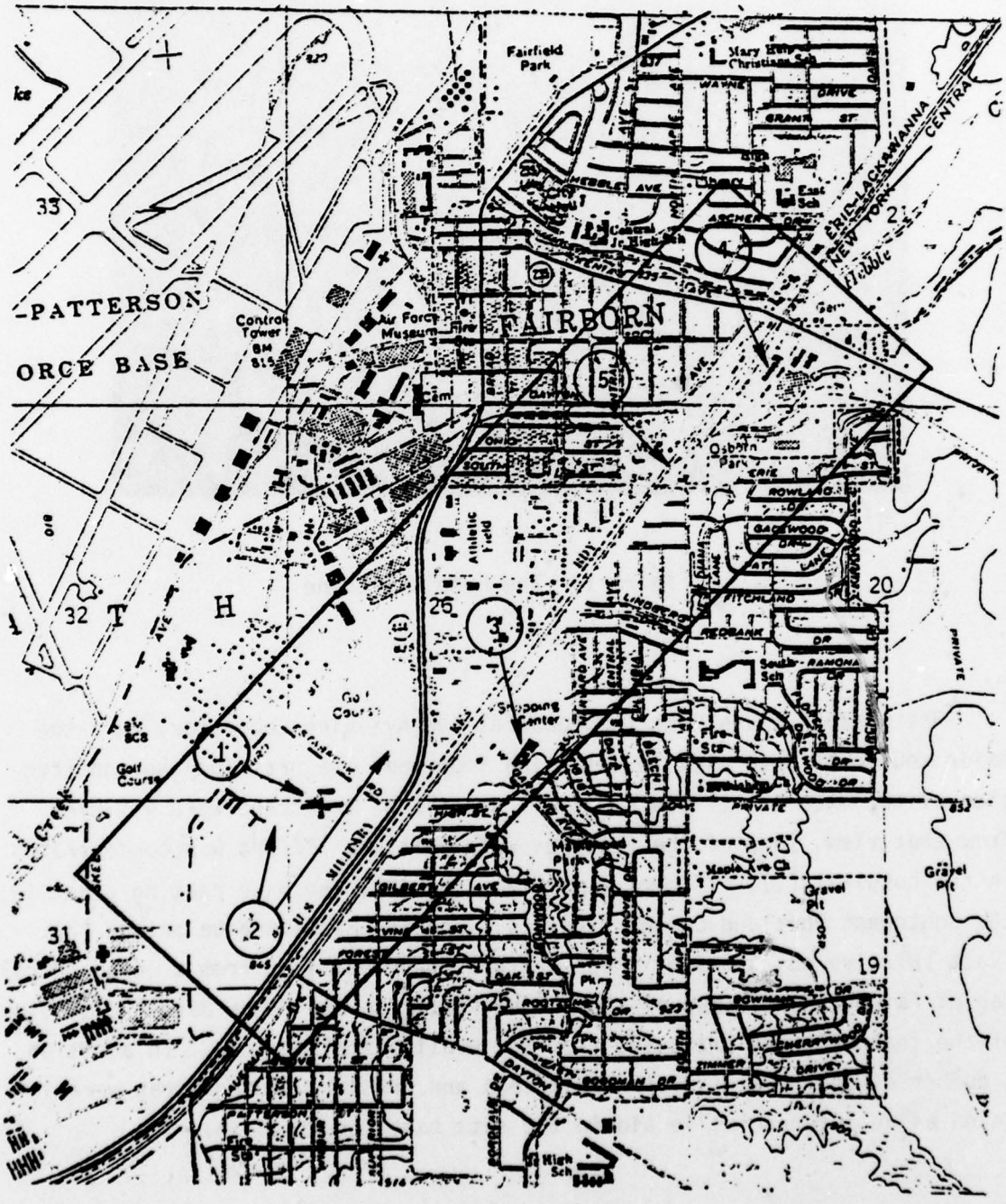

Figure 2. Geographical Map of the Section Selected for the Model

A data base was prepared for the chosen scene at each of three levels of detail. These correspond to levels IA, IIA, and IIIB of the 1974 DMAAC specification. Level IA has a resolution of 500 feet, level IIA has a resolution of 200 feet, and level IIIB has a resolution of 50 feet. The data bases for these three resolutions were prepared in accordance with guidelines in "Specifications for Digital Radar Landmass Simulator."

2.2 DATA BASE CONSTRUCTION

2.2.1 Level IA

For level IA, only 12 features were modeled and their "feature analysis data table" is included in Figure 3. Dimensions of the hospital, the steam plant, and the cement plant fell below the minimum requirement of 500 ft height and width for level IA and, therefore, were not modeled to scale. Instead, they were modeled as point features, with diameters the same as their convex covers, as suggested by the "isolated structures criteria" (100 ft across and 500 ft distant from other groupings).

Each of the two groups of visible family duplexes on the base were modeled as homogeneous blocks of uniform height, since the dimensions of individual houses fell below the minimum size criterion for level IA.

All of the features were modeled as three-dimensional polyhedra with a base outline as indicated in Figure 4. The remaining two features are Route 4 and a ground plane, both of which are modeled as planes. The equivalent sensor data base for level IA consists of 111 surfaces consisting of 188 vertices and 544 edges.

2.2.2 Level IIA

At level IIA, 21 features met the resolution requirements. Their feature analysis data table is shown in Figure 5. Six isolated features were modeled with their basic outlines (as opposed to point features). These were the officers housing unit modeled to scale,

	A	B	C	D	E	F	G	H	I	J	K
	FAC NUMBER	FEATURE TYPE	SURFACE MATERIAL	HEIGHT	NO. OF STRUCTURES	TREE COVERAGE (%)	ROOF COVERAGE (%)	FEATURE ID	DIRECTIVITY	DIMENSION OF POINT FEATURES	LEVEL
TREES	1	2	5	40	1	80	5	907	-	-	1
CLUSTER OF FAMILY HOUSES	2	2	4	25	11	30	30	730	-	-	1
HOSPITAL	3	0	3	65	-	0	100	730	-	-	1
CLUSTER OF FAMILY HOUSES	4	2	4	25	11	30	30	730	-	-	1
STEAM PLANT	5	0	3	55	-	0	100	120	-	100	1
TREES	6	2	5	40	1	80	5	907	-	-	1
RESIDENTIAL AREA	7	2	4	25	11	30	30	400	-	-	1
RESIDENTIAL AREA	8	2	4	25	11	30	30	400	-	-	1
CEMENT PLANT	9	0	3	70	-	0	100	120	-	600	1
TREES	10	2	5	40	1	80	5	907	-	-	1
FREEWAY	11	1	6	0	-	0	0	230	-	100	1
NORMAL SOIL	12	2	10	0	1	10	5	904	-	-	1

Figure 3. Level IA Feature Analysis Code (FAC) Sheet

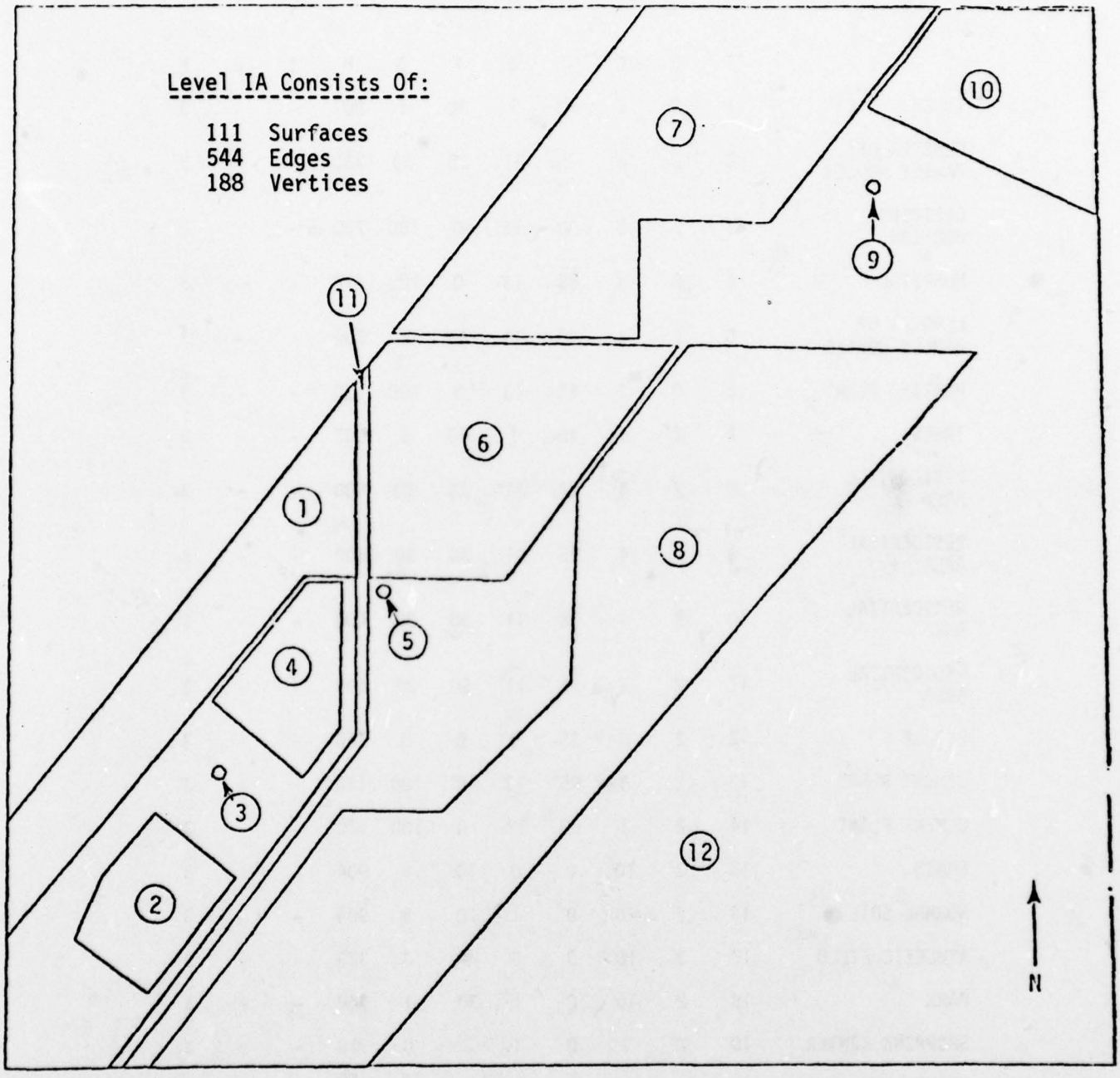

Figure 4. Outlines of Features at Level IA

	A	B	C	D	E	F	G	H	I	J	K
TREES	1	2	5	40	1	80	5	907	-	-	3
CLUSTER OF FAMILY HOUSES	2	2	4	25	11	30	30	730	-	-	3
OFFICERS HOUSING	3	2	3	40	13	0	100	730	-	-	3
HOSPITAL	4	2	3	65	13	0	100	730	-	-	3
CLUSTER OF FAMILY HOUSES	5	2	4	25	11	30	30	730	-	-	3
HEATING PLANT	6	2	3	55	13	0	100	120	-	-	3
TREES	7	2	5	40	1	80	5	907	-	-	3
RESIDENTIAL AREA	8	2	4	25	11	30	30	400	-	-	3
RESIDENTIAL AREA	9	2	4	25	11	30	30	400	-	-	3
RESIDENTIAL AREA	10	2	4	25	11	30	30	400	-	-	3
RESIDENTIAL AREA	11	2	4	25	11	30	30	400	-	-	3
BRIDGE	12	2	3	35	0	0	0	260	-	-	3
CEMENT PLANT	13	2	3	85	13	0	100	120	-	-	3
CEMENT PLANT	14	2	3	85	13	0	100	120	-	-	3
GRASS	15	2	10	0	0	10	5	904	-	-	3
NORMAL SOIL	16	2	10	0	1	10	5	904	-	-	3
ATHLETIC FIELD	17	2	10	0	0	0	0	320	-	-	3
PARK	18	2	10	0	1	30	1	900	-	-	3
SHOPPING CENTER	19	2	3	0	1	0	0	310	-	-	3
NORMAL SOIL	20	2	10	0	1	10	5	904	-	-	3
STREETS	21	2	6	0	0	0	0	200	-	-	3

(See Figure 3 for Column Headings)

Figure 5. Level IIA FAC Sheet

the lower level of the hospital with predominant height of 25 ft, the upper level on top of the lower level with predominant height of 64 ft, the heating plant, and the two largest sections of the cement plant (the kiln, finish mills, and rock storage as one and the silos and pack house as another). The sixth isolated structure is the Maple Avenue overpass. Its dimensions (420 by 60 ft) fell within the minimum requirements for level IIA, and the overpass was thus modeled to scale.

However, the shape of the bridge did not conform to the DMAAC specifications. It is supported on both ends by an earth embankment which fell below minimum size requirements for level IIA, and its shape cannot be modeled as a set of surfaces parallel (or perpendicular) to the ground plane. This accounts for the "floating in the air" effect the modeled bridge has.

Some difficulties were also encountered when modeling the lower portions of the hospital. The height differential of the terrain has the effect of an additional floor being exposed on the west side of the structure; whereas, it is covered on the east side.

Remaining features are homogeneous blocks of residential areas, tree covered areas, a park and an athletic field, two bare ground areas, and the base plane. Outlines of all the features in level IIA are shown in Figure 6, and the areas between the homogeneous blocks give outlines of the major roads. Altogether, the model at level IIA consisted of 131 surfaces constructed from 611 edges and 285 vertices.

2.2.3 Level IIIB

Level IIIB contains a data base with the finest level of detail. Again, features were selected from the single view from the tower and do not include all the detail allowed by DMAAC specifications. Despite that, there were 87 individual features (some of which had several parts). The feature analysis sheet is shown in Figure 7. The first 37 features were the family duplexes on the Air Force Base grounds. Most of the

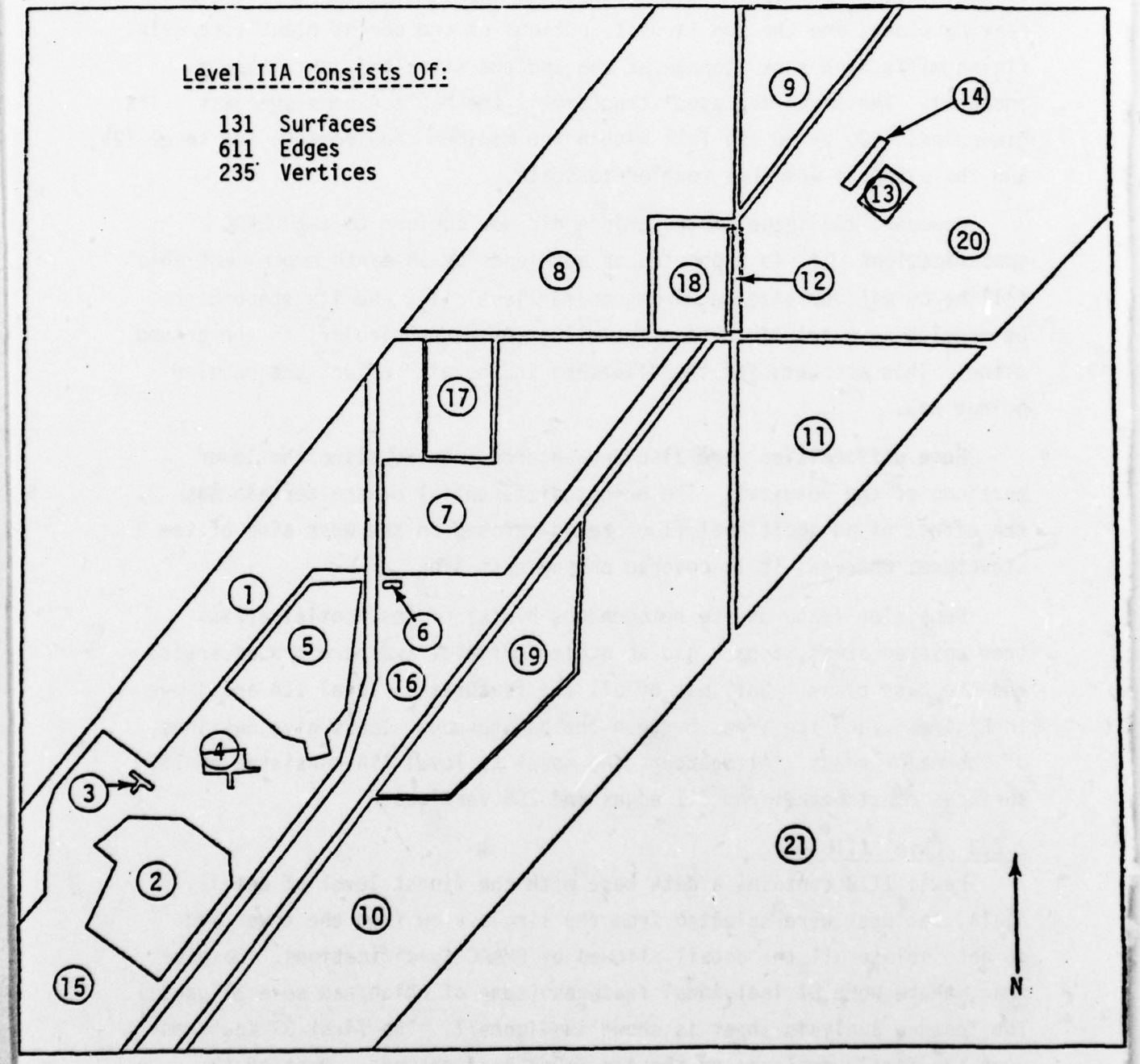

Figure 6. Outline of Features at Level IIA

	A	B	C	D	E	F	G	H	I	J	K
	FAC NUMBER	FEATURE TYPE	SURFACE MATERIAL	HEIGHT	NO. OF STRUCTURES	TREE COVERAGE (%)	ROOF COVERAGE (%)	FEATURE ID.	DIRECTIVITY	DIMENSION OF POINT FEATURES	LEVEL
FAMILY HOUSING	1-22,25-39	2	4	25	11	30	30	730	-	-	6
OFFICERS HOUSING	23	2	3	40	13	0	100	730	-	-	6
HOSPITAL	24	2	3	65	13	0	100	730	-	-	6
HEATING PLANT	40	2	3	55	13	0	100	120	-	-	6
SERVICE STATION	41	2	4	25	10	0	100	300	-	-	6
CHURCH	42	2	4	25	10	0	100	620	-	-	6
BRIDGE	43	2	3	35	0	0	0	260	-	-	6
CEMENT PLANT	44-55	2	3	85	13	0	100	120	-	-	6
TREES	56-62	2	5	40	1	0	5	907	-	-	6
RESIDENTIAL BLOCKS	63-75	2	4	25	11	30	30	400	-	-	6
GRASS	76-80	2	10	0	0	10	5	904	-	-	6
PARK	83	2	10	0	0	30	1	900	-	-	6
BARE GROUND	81-82,84-86	2	10	0	1	10	5	904	-	-	6
STREETS AND ROADS	87	2	6	0	0	0	0	200	-	-	6

Figure 7. Level IIIB FAC Sheet

individual houses were not far enough apart to satisfy the DMAAC "isolated structure criteria" (50 ft apart). Instead, they were combined into groups running parallel to the streets. The rooftops of the duplexes are the major visible part of the group of housing on the Air Force Base; however, since the specifications do not allow for sloped roofs, the model does not accurately reflect them.

Feature 23 is the "officers quarters" building, which was modeled to scale. The hospital (feature 24) was modeled as four separate levels with heights of 96 ft, 64 ft, 32 ft, and 25 ft, as suggested in DMAAC "Height Continuity Specifications." Terrain elevation presented difficulties for the bottom level as they did during the construction at level IIA.

Although the metal shades over the southwest walls of the hospital were quite noticeable on the photographs of the scenes, they were not included in the model. This was done since the specifications do not have clear instructions for modeling significant details on sides of buildings. All the features can only be modeled as DMAAC "areas with predominant height."

The heating plant, service station, and church of Kauffman and Powell Avenues were modeled to scale (features 40, 41, 42). The Maple Street overpass was modeled as in level IIA and with the same assumptions (feature 43). The cement plant was divided into 11 individual structures, each of which had outlines to scale: (44 - silos, 45 - pack house, 46 - warehouse, 41 - water tower, 48 - smokestack, 49 - precipitator, 50 - kiln building, 51 - finish mills, 52 - rock storage, 53 - laboratories and offices, 54 - shops and stores, and 55 - railroad tracks).

Again, much of the significant detail was not modeled since specifications do not allow for sloped roofs or detail on the sides of the buildings. Furthermore, the rock storage building is a structure with a sloped roof and without one wall; thus, its model does not reflect its actual shape.

Remaining features are homogeneous blocks of either residential areas or tree-covered areas, grass patches, and bare dirt fields. As in level IIA, the base plane is covered by the homogeneous areas so as to form outlines of the major streets, Figure 8. The level IIIB data base consisted of 684 surfaces made out of 3203 edges and 1155 vertices.

2.2.4 Material Data Base

As stated in the introduction, the approach taken in this study was to determine what information is needed to simulate the imagery in the handbook. This required the derivation of a tonal model for the simulation of passive sensor imagery. The tonal model will be described in Section III. What is of concern in this section is the additional data base descriptors required by the tonal model.

For each of the sensors, various surfaces in the geometrical data base will attain different shades depending on the physical properties of the surfaces they represent. For the LLLTV simulation, only the surface reflectivity close to the visible band is used during the shade assignment. For the FLIR model, not only is the surface condition important, but the composition of walls belonging to the surface is also necessary. This additional information was added to the data base. A list of available surface material types is shown in Figure 9. To completely describe the hospital scene, the material type and reflectivity of each surface in the scene had to be incorporated in the data base. This was done through a four-digit word. The first two digits are the material type and the last two digits are the percent reflectivity. The additional feature description is given in Figure 10 for each feature in the data base for levels IA, IIA, and IIIB. For example, the walls of the officers housing, feature 23 at level IIIB, has a code 2040, meaning they are made of brick, which is 40% reflective at the visible bands.

The need for these additional data base descriptors and their use will now be described in the discussion and derivation of the thermal model.

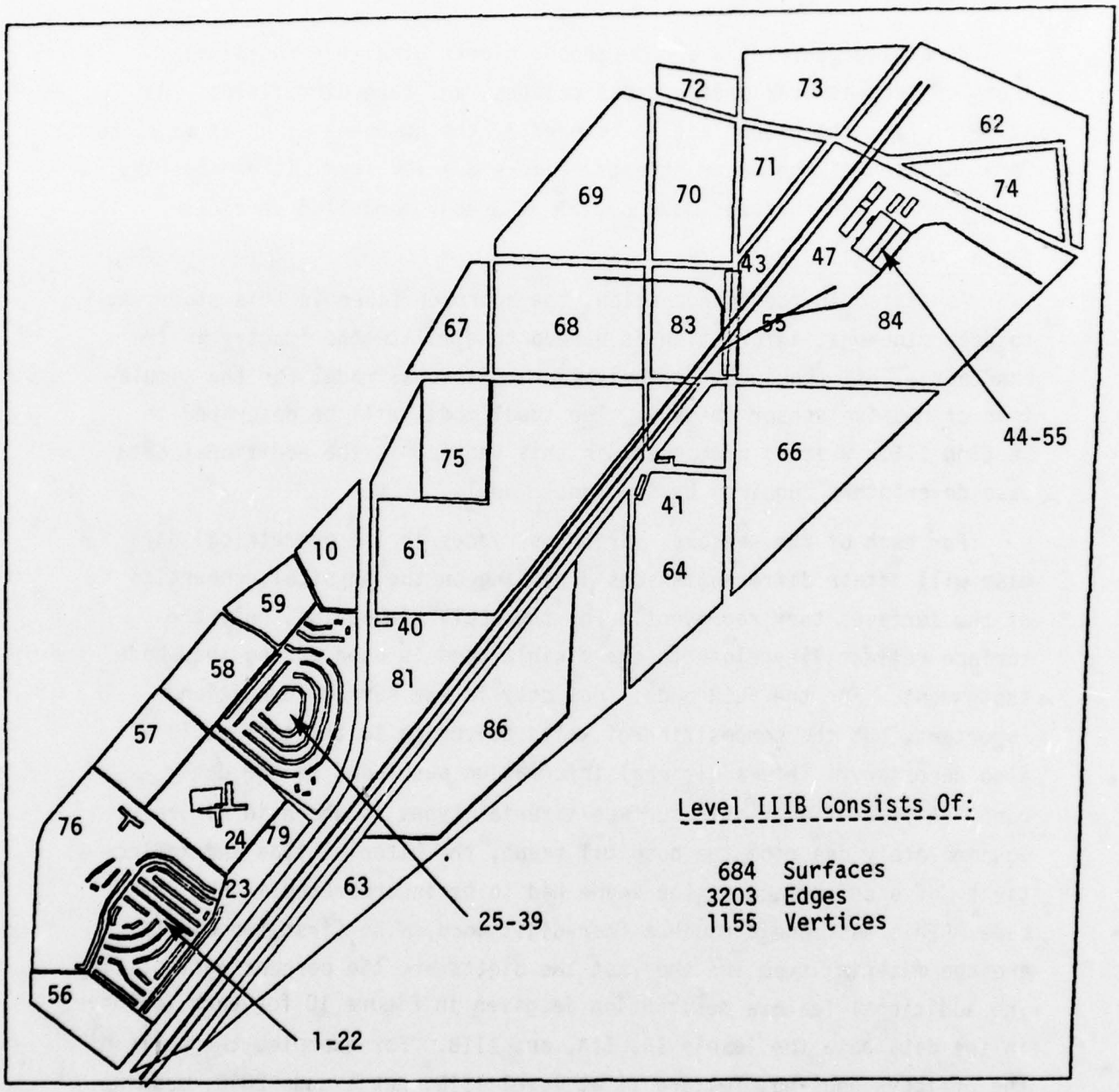

Figure 8. Level IIIB FAC Numbers

Siding

1 Asphalt Shingle
2 Asphalt Paper
3 Asbestos Shingle
4 Flat Asbestos
5 Lapped Wood
6 Flat Wood
7 Vertical Sine - Corrugated Metal
8 Vertical Square - Corrugated Metal
9 Horizontal Sine - Corrugated Metal
10 Horizontal Square - Corrugated Metal
11 Lapped Metal
12 Flat Metal
13 Rough Stucco
14 Smooth Stucco
15 Corrugated Plastic
16 Smooth Plastic

Masonry

20 Brick
21 Textured Brick
22 Concrete Block
23 Textured Concrete Block
24 Sandblasted Concrete
25 Smooth Concrete
26 Textured Concrete
27 Stone
28 Clay Tile
29 Textured Clay Tile

Homogeneous Blocks

30 Residential
31 Inner City
32 Industrial
33 Natural

Glass

40 1/4" Clear
41 1/2" Clear
42 3/4" Clear
43 1/4" Tinted
44 1/2" Tinted
45 3/4" Tinted
46 Screen

Shingles

50 Asphalt
51 Asbestos
52 Wood
53 Clay Tile
54 Slate
55 Transite

Roof

60 Corrugated Galvanized
61 Corrugated Plastic
65 Copper Sheet
66 Asphalt
67 Built-up (paper, tar, stones)

Pavements

80 Concrete
81 Asphalt

Grounds

90 Bare Earth
91 - sand
92 - clay
93 - loam
Grass
94 - cut
95 - long

Trees

96 Deciduous
97 Coniferous
98 Water

Figure 9. Currently Available Material Types

FEATURE NUMBER	FEATURE DESCRIPTION	MATERIAL TYPES ROOF MATERIAL	MATERIAL TYPES WALL MATERIAL
	LEVEL IA		
1,6,10	Trees	3314	3310
2,4,7,8,9	Residential Suburban	3030	3630
3	Commercial	3430	3434
5,9	Industrial	3230	3238
11	Roads	8038	8038
	LEVEL IIA		
1,7	Trees	9614	9610
2,5,8	Suburban Residential	3030	3030
3	Residential Inner City	3130	3130
4	Government Buildings	3430	3430
6	Industrial (Heating Plant)	3230	3245
12	Industrial (Bridge)	3230	3238
12-14	Industrial (Cement Plant)	3230	3238
15,16,17,18,19,20	Terrain	3320	3320
21	Roads	8038	8038

Figure 10. List of Features and Their Material Types

FEATURE NUMBER	FEATURE DESCRIPTION	MATERIAL TYPES ROOF MATERIAL	WALL MATERIAL
	LEVEL IIIB		
1-22	Individual Houses	5030	2040
23	Officers Housing	6730	2040
24	Hospital	6730	2636
25-39	Individual Houses	5030	2040
40	Heating Plant	6730	2245
41	Service Station	6730	1040
42	Church	5030	2060
43	Bridge	8038	1230
44	Cement Plant Silos	1230	2530
45	Cement Plant Pack House	6730	2240
46	Cement Plant Warehouse	6730	2240
47	Cement Plant Water Tower	1230	1230
48	Cement Plant Smokestack	2000	2040
49	Cement Plant Precipitator	6730	2040
50	Cement Plant Kiln Building	6730	2640
51	Cement Plant Finish Mills	0930	0940
52	Cement Plant Rock Storage	1220	1210
53	Cement Plant Laboratories & Offices	6730	2025
54	Cement Plant Shop & Stores	6730	2025
55	Cement Plant Railroad Tracks	1220	1220
56-62	Trees	9614	9610
63-75	Residential Blocks	3040	3040
76-80	Grass	9420	9420
83	Park	9523	9523

Figure 10. (Continued)

III. TONAL MODEL DEVELOPMENT

This section presents the electromagnetic and thermal models used to produce LLLTV and FLIR sensor imagery. It shows the overall model consisting of a scene, environment, and sensor as implemented in a software system.

3.1 THERMAL MODELING

A thermal model is the central part of the passive infrared (IR) simulation [2]. Thermal sources in the exterior environment and interior of objects are considered by this model. Thermal paths from sources to surfaces link the exterior and interior environments to each surface in the scene. A finite difference model of the cross section of each surface (typically a flat slab), with the environment paths as boundary conditions, completes the thermal model.

3.1.1 Modes of Heat Transfer

There are three modes of thermal transport. They are conduction, convection, and radiation. These are only statistically understood phenomena in that they are the result of a large number of statistically measurable elemental processes. For present purposes, it is necessary only to understand where each path occurs and how to characterize each.

Standard equations for each thermal transport method are used in the developed thermal model. For conduction in homogeneous stationary media, the equation of thermal transport in a three-dimensional Cartesian coordinate system is

$$\frac{\partial^2 T}{\partial x^2} + \frac{\partial^2 T}{\partial y^2} + \frac{\partial^2 T}{\partial z^2} = \frac{c}{K} \frac{\partial T}{\partial t} \qquad (1)$$

where "K" is a constant thermal conductivity, "c" is a constant capacity per unit volume, "T" is the temperature at (x,y,z,t), and "t" is time. The thermal model deals only with thermal conduction across a flat slab in one dimension; hence, the conduction equation reduces to

$$\frac{\partial^2 T}{\partial x^2} = \frac{c}{K} \frac{\partial T}{\partial t} \tag{2}$$

This differential equation lacks boundary conditions. These conditions are convective air and radiative heat loadings from the exterior and interior environments, plus an initial temperature cross section in x. This leads to the equations of convective and radiative transport.

For convective transport across a planar surface at x = 0, the equation is

$$\bar{h}(T_{amb} - T(0,t)) = c \frac{\partial T(0,t)}{\partial t} \tag{3}$$

where $\bar{h}$ is the average convection conductance per unit surface area. The term $\bar{h}$ is a derived coefficient based on surface conditions and convection. It is the cumulative effect of wind speed and direction relative to the surface orientation, surface size, etc. The approach used here is to assign a value based on ideal conditions such as laminar or turbulent flow combined with standard formulae using Reynolds and Nusselt numbers. Feature shape, surface type and orientation, and environmental conditions determine these parameters.

For radiative transport across a planar surface at x = 0, the equation is

$$\sum_{i=1}^{N} (\alpha_i E_i) - \varepsilon_T \sigma T^4 = c \frac{\partial T(0,t)}{\partial t} \tag{4}$$

where there are "N" sources of irradiant power "E_i", "ε_T" is the average thermal emittance, "α_i" is the average absorption for irradiant energy of "i's" spectrum, and "σ" is the Stefan-Boltzmann constant.

3.1.2 The Viewing Factor

The characterization of radiant paths requires a measure of energy exchange: the viewing factor. The viewing factor is used when two surfaces radiate to each other and one wants to calculate the amount of energy interchanged. The amount of energy reaching surface 2 from surface 1 can be calculated as follows.

Surface S_1 is characterized by its diffuse radiance. For each differential element dS_1, a portion of the radiant energy hits surface S_2. This part of the radiant energy of surface S_1 has to be summed in order to compute the radiant interchange between them. This summation can be characterized by the equation

$$F_{1\to 2} = \frac{1}{A_1} \int\int \frac{\cos \theta_1 \cos \theta_2}{\pi r^2} \, dA_1 \, dA_2 \qquad (5)$$

where "θ_i" is the angle between the normal to dA_i and the line segment connection dA_1 and dA_2, "r" is the length of the line segment connecting dA_1 and dA_2, and "A_i" is the area of surface S_i. The shape factor is used in radiant interchanges where the surfaces have constant radiance across themselves as viewed by each other. In such a case, where the radiance of surface S_1 is L_1 and the radiance of surface S_2 is L_2 (as viewed by each other), the shape factor is used to calculate the net radiant interchange by

$$L_{S_1 \to S_2} = \pi L_1 \, A_1 \, F_{1\to 2} \qquad (6)$$

$$L_{S_2 \to S_1} = \pi L_2 \, A_2 \, F_{2\to 1} \qquad (7)$$

For thermal modeling, the shape factor can be used with surface temperature to compute heat loading power by

$$Q_{1\to2} = \varepsilon\sigma T^4 A_1 F_{1\to2} \qquad (8)$$

The above procedure demonstrates how radiant paths are modeled in the finite difference thermal model.

3.1.3 Environment Paths

A simplified environmental model is used. Figure 11 presents a schematic of the model. The ground plane, sky hemisphere, sun, and the four diffuse solar quadrants are the exterior radiant paths to a surface. The atmosphere is the exterior convective path to a surface. The interior side of a surface has a free convection path to the interior air and a radiation path.

The ground plane is a horizontal plane of infinite extent with constant diffuse thermal radiance. It is a grey body with a spectral peak near 10 microns. Its diffuse radiance is related to temperature by Stefan-Boltzmann's Law. The ground can be dry, wet, or snow covered. Under wet and snow covered conditions, it closely approximates a black body, so the ground condition does not have major impact on its thermal emission. When the ground is snow covered, though, its maximum temperature is 32°F.

The sky is a hemisphere over the ground plane. It is a close approximation to a black body except in spectral bands where the sky is highly transparent. It has constant radiance over the hemisphere because almost all the received thermal energy is from the bottom 1 kilometer of the sky. The sky's spectral peak is near 10 microns. The presence of clouds, especially low, rain-bearing clouds, increases the sky's radiant, or

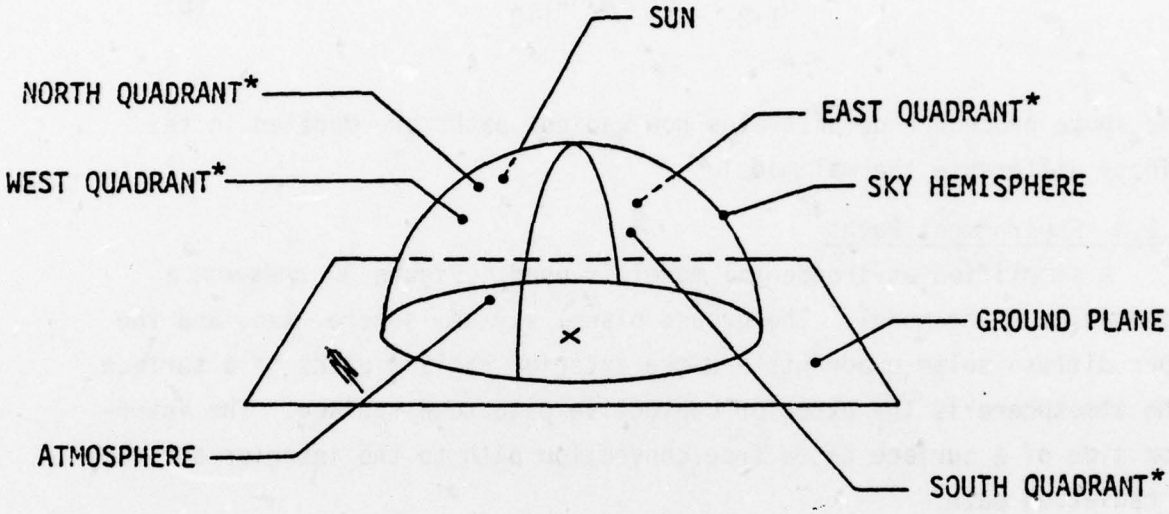

*The N, E, S, W quadrants are diffuse solar radiant surfaces.

Figure 11. Schematic Representation of Exterior Environment

apparent, temperature because clouds are opaque in those bands where the sky is highly transparent. The sky and ground have similar thermal emission bands since their temperatures are similar.

The sun is a 5900°K black body. It is a source of both direct and diffuse radiation. The direct radiance is modeled as being emitted by a point source, while the diffuse radiance is modeled as coming from four sky quadrants. Each quadrant is a constant radiance diffuse surface that approximates the diffuse solar radiation falling from that quadrant of the sky. The spectral distribution of solar radiation is significantly different from that of ground and sky. About 99 percent of solar radiation is between 0.2 and 3.0 microns which contains the visible wavelengths. However, the bulk of the received radiation from the ground and sky is at wavelengths greater than 3 microns.

The atmosphere is modeled as a gas. Its temperature and wind vector determine the rate of convection between a surface's exterior and the atmosphere. Reynolds and Prandtl numbers are used to estimate convection rate. Precipitation influences exterior heat transfer since incident water is heated by conduction to the surface temperature. Based on precipitation rate, wind vector, and surface orientation, a certain quantity of water hits a square meter of surface per hour. This water is heated from its percipitation temperature to the surface temperature, with a resulting heat transfer and evaporation.

The interior side of a surface has a free convection path to the interior air. The interior air may be air conditioned (i.e., in the range 65° to 75°F), heated (i.e., kept above 65°F), unheated (i.e., enclosed but not heated or cooled), or open to the outside. Based on the condition of the interior air, free convection from the interior surface to the enclosed air mass can occur.

3.1.4 The Finite Difference Model

The geometric description of objects for the thermal model consists of a set of points, line segments, and planar polygonal-bounded surfaces. Each is modeled as either a flat layered slab, a cylinder, or a sphere. Periodic layers like beams or studs can be modeled. Layers are sectioned with thermal capacity within the section and thermal resistance to the adjacent sections assigned. The edges of the slab form the boundary of the slab with its exterior and interior environments. Boundaries or edge effects between different wall cross sections are ignored. This is the basis of the finite difference model.

The finite difference method is a powerful method of approximating many types of partial differential equations. Applied to thermal modeling, the method permits quantitative computer modeling of the walls, roof and ceiling, and also interior and exterior convective and radiative interactions of a target feature.

Figure 12 shows three typical wall cross sections: uninsulated wood, insulated wood, and brick. The wall models interface with the environment at their interior and exterior, where convective and radiative transfer occur. The interior wall models include conduction through solids and convection and radiation across air gaps. The parallel thermal paths of wood studs and either air gaps or insulation are modeled as parallel one-dimensional paths without cross paths included. This has been found satisfactory for measured cases.

The finite method has a theoretical foundation in approximation theory using function spaces. The theory of application has been developed and includes criteria for a well-formulated model in terms of consistency, convergence, and stability. A finite difference equation (F.D.E.) can be written for a node "i" connected to two other nodes in the model:

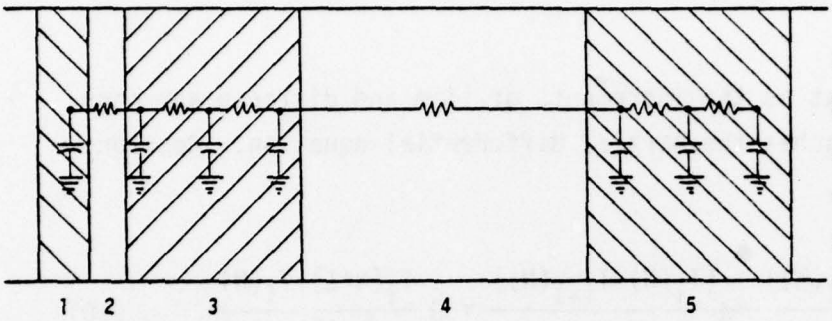

1. ¼" Asphalt Paper
2. 1/100" Air Space
3. 3/4" Plywood
4. 4" Air Space
5. ½" Gypsum Board

Uninsulated Wood Wall

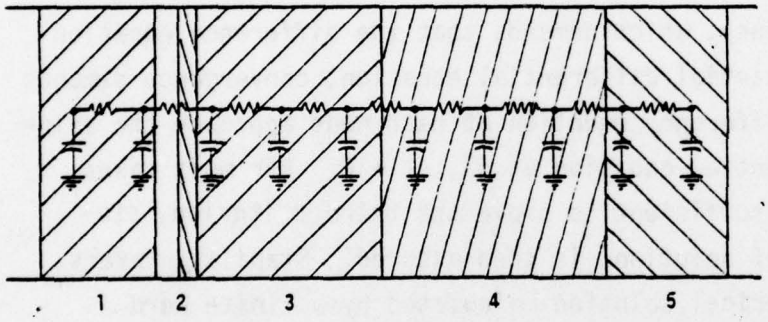

1. 5/8" Wood Siding
2. Building Paper & 2/100" Air Space
3. 3/4" Plywood
4. R-11 Insulation Batting
5. ½" Gypsum Board

Insulated Wood Wall

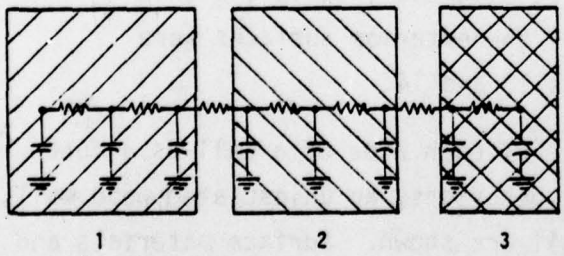

1. 4" Face Brick
2. 4" Common Brick
3. 3/4" Plaster

Brick Wall

Figure 12. Three Sample Wall Cross Section and Finite Difference Models

$$T_i(N+1) = T_i(N)\left(1-2\left(\frac{\Delta tk}{c\Delta x^2}\right)\right)+ \frac{\Delta tk}{c\Delta x^2}\ T_{i-1}(N) + T_{i+1}(N) \qquad (9)$$

Consistency demands that as the increments of time and distance approach zero, the F.D.E. approaches the partial differential equation. Rearranging (9), we see that

$$\frac{(T_{i+1}(N)-T_i(N)) - (T_i(N)-T_{i-1}(N))}{\Delta X^2} = \frac{c}{K}\frac{T_i(N+1)-T_i(N)}{\Delta t} \qquad (10)$$

As ΔX, $\Delta t \to 0$, this approaches the differential equation for conduction. As contrasted with consistency, which demands that the difference equation at each node approach the partial differential equation, convergence demands that the solution of the difference equation at each node approach the solution to the partial differential equation at ΔX, $\Delta t \to 0$. For most cases of thermal modeling, it is sufficient to prove the third criterion, stability, since convergence of solutions is then assured. Stability refers to the behavior of the numerical solution calculated by a finite word length computer. The stability criterion guarantees that the truncation errors of iterating the F.D.E. do not propagate.

Using the model, the temperature at discrete intervals within a wall and the heat flow from (or into) the exterior surfaces were computed and are illustrated in Figures 13 and 14.

Figure 13 presents the temperature of each node of a wall as a function of time. For contrasting thermal behaviors, an uninsulated wood wall, an insulated wood wall, and a brick wall are shown. Surface materials and their cross sections have a major impact on exterior surface temperature.

Figure 14 presents the thermal loading of three different environments as a function of time for some standard surface orientations. The environment, time, and surface orientation all have significant impact on thermal exchange at the surface.

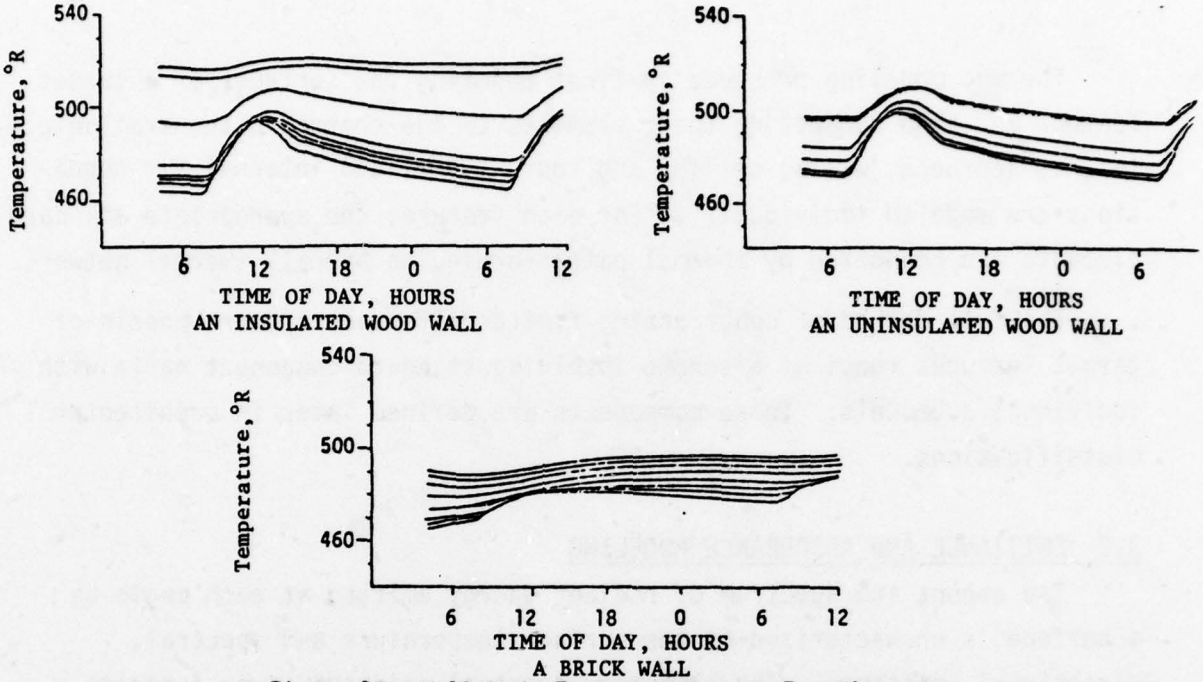

Figure 13. Wall Node Temperature as a Function of Time for an E-S-E Facing Wall on 7 February

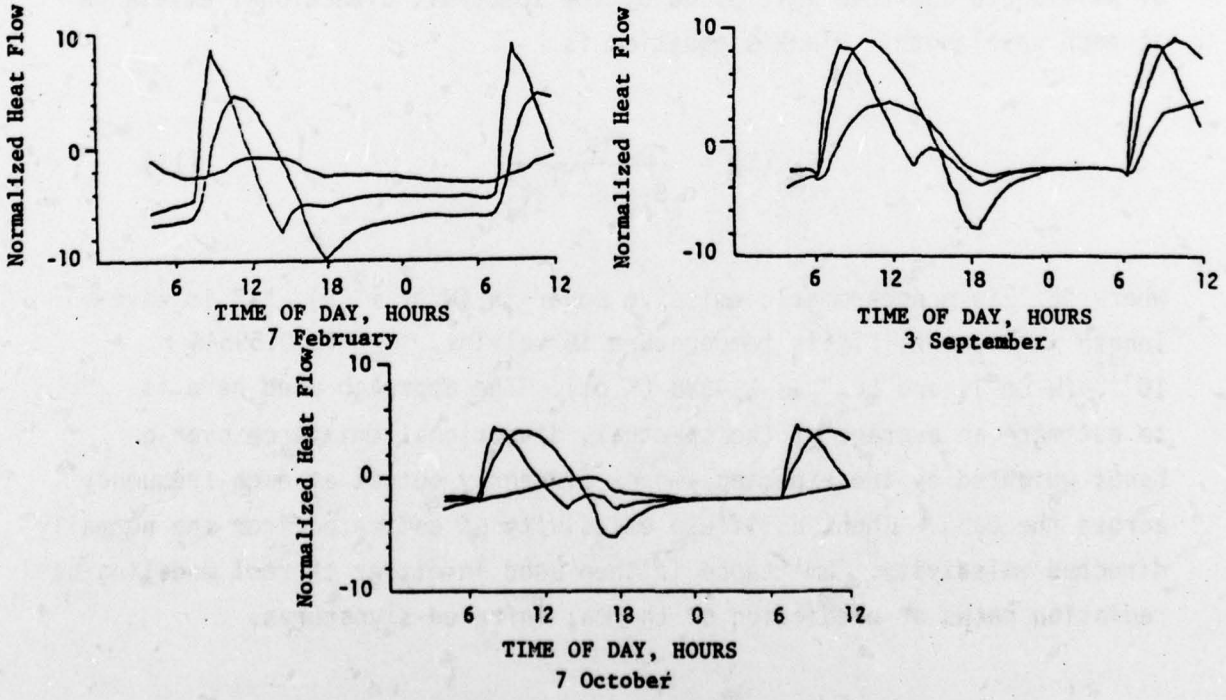

Figure 14. Environmental Thermal Loading as a Function of Time

Thermal modeling proceeds by first modeling the surfaces of a target feature and then connecting these elements to the thermal paths available. In this approach, walls, ceiling and roof, floor, and internal air conditions are modeled individually. For each feature, the appropriate standard elements are connected by thermal paths forming an overall thermal network.

The full method of constructing finite difference network models of target features requires a scheme involving standard component parts with individual submodels. These components are defined later in architectural classifications.

3.2 EMITTANCE AND ABSORBANCE MODELING

The amount and spectrum of radiant energy emitted at each angle by a surface is characterized by the surface temperature and spectral, *directional emittance. The blackbody spectral emissive power function* of Plank is used to calculate the maximum emissive power as a function of wavelength and then multiplied by the spectral, directional emittance at each wavelength. Plank's equation is

$$E_{b\lambda}(T) = \frac{c_1}{\lambda^5(e^{c_2/\lambda T} - 1)} \qquad (11)$$

where "E_b" is monochromatic emissive power in (W/hr m^2 μ), "λ" is wavelength in microns, "T" is temperature in kelvins, "c_1" is 0.59544 x 10^{-12} (W cm^2), and "c_2" is 1.4388 (K cm). The approach used here is to estimate an average of the spectral, directional emittance over a band, weighted by the expected amount of energy output at each frequency across the band. Then, a diffuse emissivity is estimated from the normally directed emissivity. Emittance is then used in either thermal modeling of radiation paths or prediction of thermal infrared signatures.

Emittance is a statistical property not completely determined by the surface material. Surface conditions, including roughness and degree of oxidation, have a major impact on emittance. The volume of material just under the surface also contributes to emittance in nonconductors. Figure 15 shows some directional emittance curves of prepared clean surfaces. The curves approximate diffuse emissive sources except near grazing angles. In addition to the amount of energy emitted, there can be a degree of polarization to the energy, especially in the millimeter band.

The basis of thermal emission modeling is Plank's law of spectral blackbody emission. From this equation several radiation laws can be derived. Integrating Plank's equation, one finds the total blackbody thermal hemispherical emission is

$$E_b = \sigma T^4 \tag{12}$$

where "σ" is the Stefan-Boltzmann constant. Wien's displacement law can be derived from Plank's equation. It is

$$\lambda_{max} \cdot T = c_3 \tag{13}$$

where "c_3" is 0.28978 (K cm).

At the temperatures of most objects on the ground, the bulk of emitted energy is longer than 6μ. There is a need to model energy reflected and absorbed in the emission band of ground features (i.e., roughly 3 to 15μ) in order to compute radiant paths for thermal modeling.

In addition to the 0.2 to 3.0μ and 3.0 to 15.0μ bands, there is a need to model emittance, absorbance, and reflectance for 0.8 to 1.1μ (LLLTV) and 8 to 14μ (FLIR) sensor bands. Emittance, absorbance, and reflectance functions are required for each spectral band of interest, i.e., those bands which are significant in describing the ground, sun, or a specific sensor.

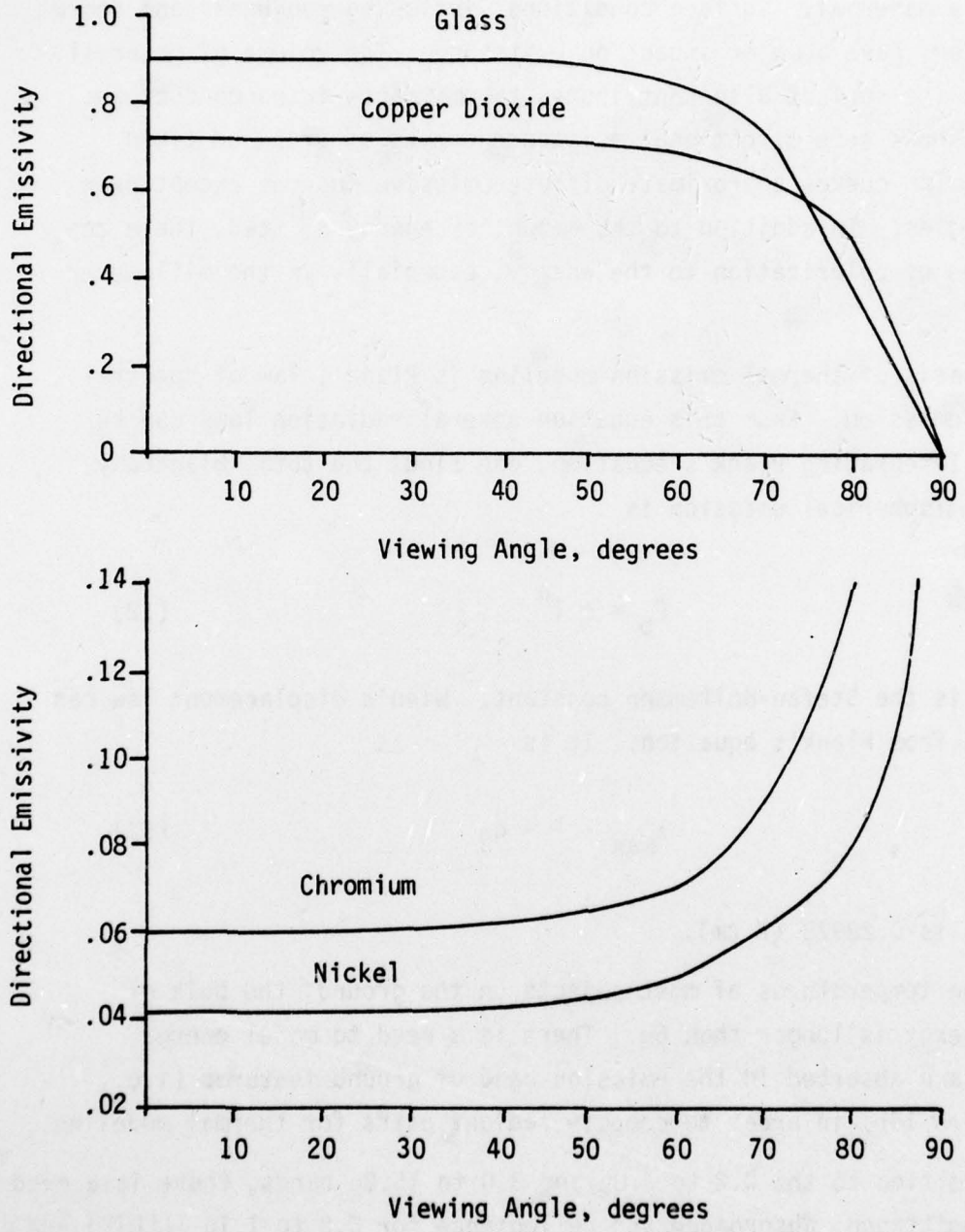

Figure 15. Directional Emissivities of Various Surfaces. (Heat and Mass Transfer by E.R.G. Eckert and R.M. Drake.Copyright 1959.McGraw-Hill Book Company, New York.)

Finally, Kirchoff's Law plays an important role here in relating emittance (ε), absorbance (α), and reflectance (ρ) functions. Kirchoff's Law equates emittance with absorbance under conditions of equilibrium. Thus, under the condition that transmittance is zero, $\alpha = \varepsilon = 1 - \rho$ and all three radiation interactions are related in each band.

3.3 REFLECTANCE MODELING

The amount of reflected radiant energy in any direction as a function of the incidence angle of the irradiant energy is characterized by the bidirectional reflectance. The bidirectional reflectance is the ratio of the incremental radiance $dL_r(\theta_i,\theta_i)$ over the incremental irradiance $dE_i(\theta_i, \theta_i)$:

$$\rho'(\theta_i,\phi_i,\theta_r,\phi_r) = \frac{dL_r(\theta_r,\phi_r)}{dE_i(\theta_i,\phi_i)} \ (Sr^{-1}) \qquad (14)$$

The bidirectional reflectance is a statistical phenomenon. Most real surfaces are too complicated to have a single constant reflectance. In these cases, the bidirectional reflectance represents only the mean reflectance for the given incidence and reflectance angles. Since there is a significant reflectance variation from point-to-point along the surface, care is necessary when interpreting measured bidirectional reflectances. One approach is to filter measured data to eliminate high frequency angular changes in reflectance since these contain much of the variable-over-the-surface information (i.e., noise).

Polarization is an important factor in reflectance behavior. Polarizations parallel and perpendicular to the plane of incidence have significantly different reflection behaviors so that after reflections, light originally unpolarized can gain a degree of polarization.

The simplest model of reflection is Lambertian (i.e., cosine law) diffuse reflection. This is a constant radiance reflection over the hemisphere above the surface. Many simulations use this simple diffuse model since it appears to be an adequate description of the scattering mechanism in many cases.

The next step, which was not within the scope of this study, is to develop a capability to include specular reflection in the model.

3.4 ATMOSPHERIC MODELING

The atmosphere interacts with radiation via scattering, absorption, and defocusing. In the model developed for this effort, defocusing has been ignored, while scattering and absorption interactions are easy to characterize by the attenuation coefficient α. When applied to a radiant surface at a range, r, the transmittance in percent is $e^{-\alpha r}$. If the surface has radiance I_s and the atmosphere has apparent radiance I_a at infinite range, the observed radiance is

$$I_o = I_s\, e^{-\alpha r} + I_a\, (1 - e^{-\alpha r}) \quad . \qquad (15)$$

This is simplifying the underlying phenomena. In order to be accurate, attenuation should be applied to radiances wavelength by wavelength to account for spectral inhomogeneities in the atmosphere. Yet, that would require a prohibitive amount of computation. When atmospheric attenuation is involved, radiant energy is computed for spectral windows, and an average attenuation rate computed over each window. When the paths are short, as between nearby surfaces, atmospheric attenuation is ignored.

3.5 A METHOD OF CHARACTERIZING ARCHITECTURAL SYSTEMS

In order to perform thermal modeling, cross sections of walls and roofs and interior air volume are needed. These components provide thermal memory. Unfortunately, it is impractical to determine the cross section of each surface in a scene.

The approach taken here is to construct standard cross sections that are labeled and can be entered into a model as required. The validity of this approach is based on all the constraints placed on building designers (and nature). Building codes, architectural methods taught in school, available construction materials, and environmental conditions all limit the types of design.

The first step is to characterize a feature's overall construction type. Figure 16 illustrates the top level of a construction classification tree for buildings. Other classification trees can be constructed for pavements, natural areas, etc. For buildings, the overall design is typically easy to observe from photography or is known via scene mensuration. Other types of construction, such as pavement or industrial processing structures, are also reasonably easy to visually identify and subsequently model thermally.

There are many subtrees of this classification scheme. Any building can be classified as either a single category or a mixture of categories, then each identified building component (i.e., walls, roofs, etc.) of the geometrical data base can be thermally modeled by a standard cross section. In this way, the total building is thermally modeled in terms of its construction, interior environment, and component surfaces.

It is possible to construct a thermal model of a feature by (1) classifying it in terms of standard categories, and (2) applying ideal material cross sections (corresponding to the named classification) to identified feature components (i.e., wall, windows, and roofs) in the geometrical data.

3.6 IMPLEMENTATION OF THE TONAL MODEL

The thermal model is performed in two processes. In these processes, the geometrical and thermal properties of individual objects in the scene are processed together with the dynamically changing environmental conditions in order to assign shade values to the external surfaces of the objects. The entire flow diagram of the thermal model implementation

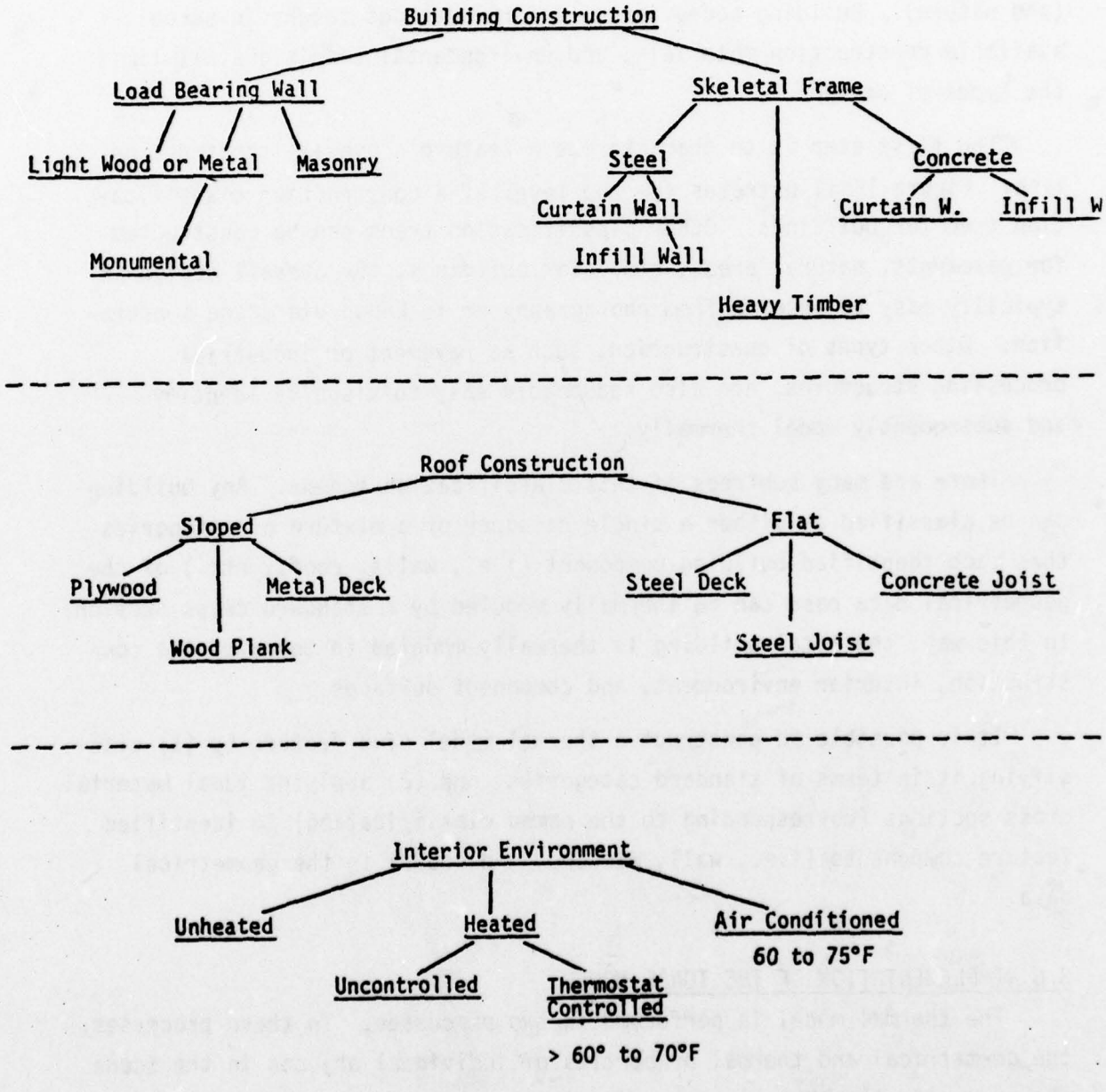

Figure 16. Basic Classification Trees for Building Systems

is shown in Figure 17. In the first process, a matrix of coefficients is constructed with an entry for each wall type in the scene. Then in the second process, each of the surfaces in the scene is assigned a shade, using the above constructed matrix.

3.6.1 Construction of a Matrix of Coefficients

For each of the available wall types (Figure 9) and each of the standard orientations, a set of four coefficients is generated. To obtain each set of the coefficients, a temperature vector is computed for five typical thermal reflectances of the current wall type. The first element of each of the five vectors is used to find a fourth degree polynomial by a least squares fit method. Coefficients of this polynomial are the next entry in the matrix of coefficients.

To allow the temperature of the wall to "catch up and settle," it is necessary to consider not only the current condition of the environment, but also the conditions of the surrounding environment during several preceding hours. Thus, the temperature vector is computed in several iterations over the time increment.

The temperature vector is set initially to have its first element equal to temperature of the interior air and is obtained from the "wall type file." The last element of the temperature vector is initially set equal to the current temperature of exterior air which is obtained from the "environment condition file," and the rest of the elements are linearly distributed between the first and last elements. Each of the elements corresponds to a "node" of the current wall type. The heat flow through the wall depends on the thermal properties of the wall and the external loading and can be analytically represented by a partial differential equation. Furthermore, using the first few terms of a Taylor polynomial for two variables, the differential equation for temperature (time, position) can be reduced to a set

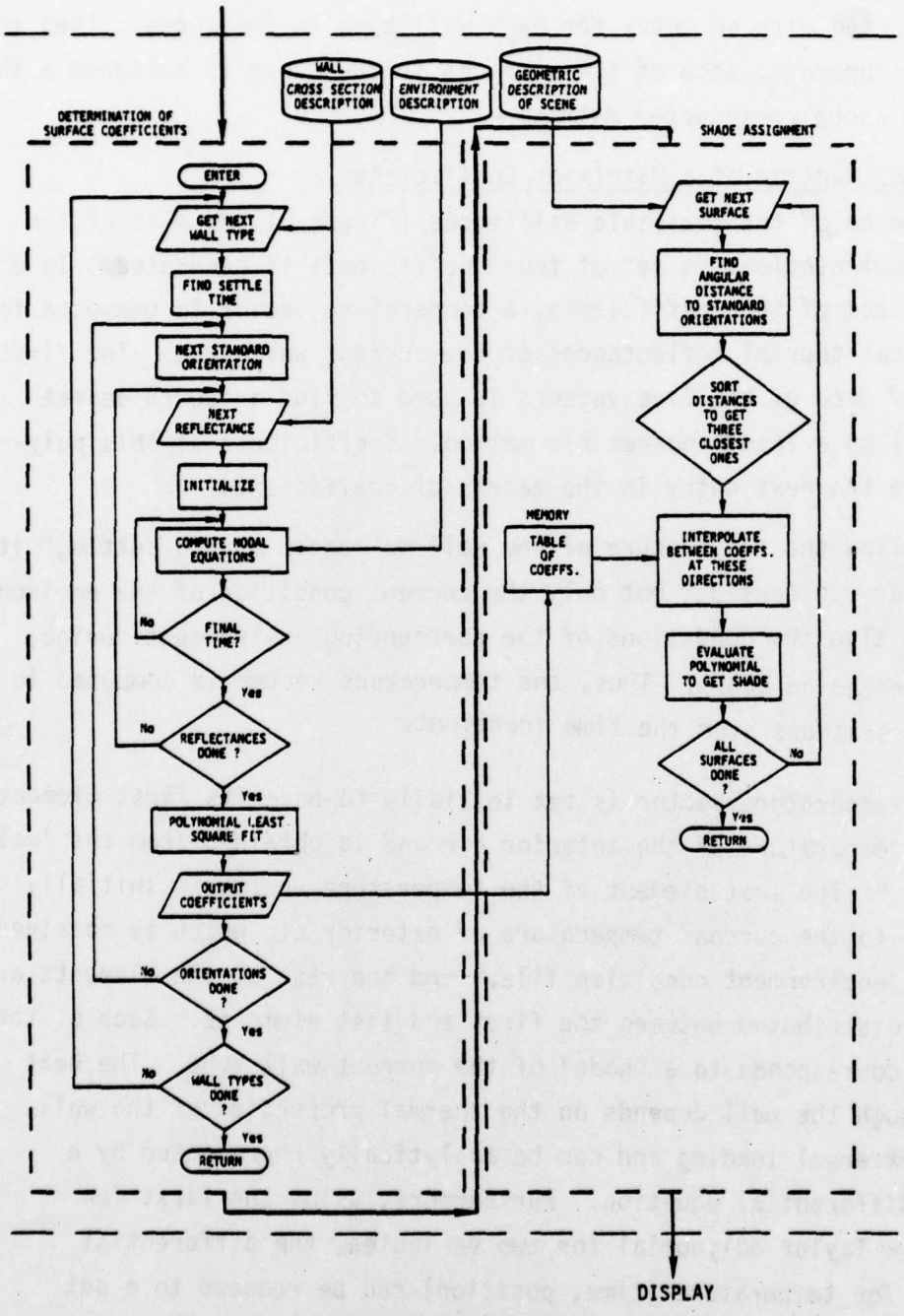

Figure 17. Tonal Model Implementation

of linear equations involving the thermal capacitance, conductance, and time increment as coefficients and temperatures at various nodes as variables. This determines a matrix, and the system of linear equations is solved by applying its inverse to the initial temperature vector. To include the influence of the change of the environment on the exterior node (surface), an extra load node is added. The load depends on:

(1) Sun position with respect to exterior surface of the wall.
(2) Amount of sky "visible" to the surface.
(3) Amount of the ground "visible" to the surface.
(4) Air temperature, wind velocity, and precipitation.

To summarize, at each time interval, a temperature vector is found where loading due to the sun, sky, and ground radiances and the air convection is added as an extra node. Such a vector is generated for each of the typical thermal reflectances of the current wall type, and the last element of these vectors is used to determine the coefficients of the fourth degree polynomial. This is done for several orientations for each of the wall types. The wall type and orientation are then used to index the matrix of coefficients.

3.6.2 Shade Assignment

Once the matrix of coefficients is constructed for a specified time of the day, the actual assignment of the shades to the individual surfaces can be performed. The wall type, the normal vector, and the thermal reflectance are serially retrieved from the geometrical data base. For each of these, the three closest standard orientations are found, since the matrix of coefficients contained only a fixed number orientations. Next, coefficients for these orientations are used to interpolate the approximate coefficients for the given orientation. Finally, a fourth degree polynomial with the approximated coefficients is evaluated at a given reflectance. This value is then properly scaled and used as the shade for the surface.

IV. IMAGE GENERATION

The scene data bases for the three different levels of detail and their construction were described in Section II, and the visual and thermal models were developed in Section III. In this section, imagery generated from the data base and the thermal/visible models and the imagery from the actual sensors are presented. Several sensitivities were selected to illustrate the effect of the changing condition of the environment on the imagery. For each of the two sensors, LLLTV and FLIR, three significantly different days were chosen to demonstrate the influence of changing seasons. The environmental conditions corresponding to the 3 days are listed in Table 1. The first of the 3 days is a cool clear day during the winter, with the direct sun radiance as the major component of the illumination and the thermal loading. The second day is a hot cloudy day during the summer, and the diffuse sun radiance (illumination by the sky) and the air temperature become more significant than on the clear day. The third day, a fall day, is an average warm day with partial cloud cover. The winter day produced the best contrast in the images. Four different times during this day were selected to illustrate the sensitivity of the scene to the diurnal variation. For this purpose images at 7 AM, 10 AM, 1 PM, and 4 PM are included for both sensors at each of the three levels of the detail.

Figure 18 shows the imagery taken from the AFHRL Sensor Handbook which are photographs of the scene taken by the actual sensors. In Section 4.2, imagery simulating the FLIR sensor is presented; imagery simulating LLLTV sensors is presented in Section 4.3. These two sections demonstrate the seasonal, diurnal, and level of detail sensitivities.

LLLTV FLIR

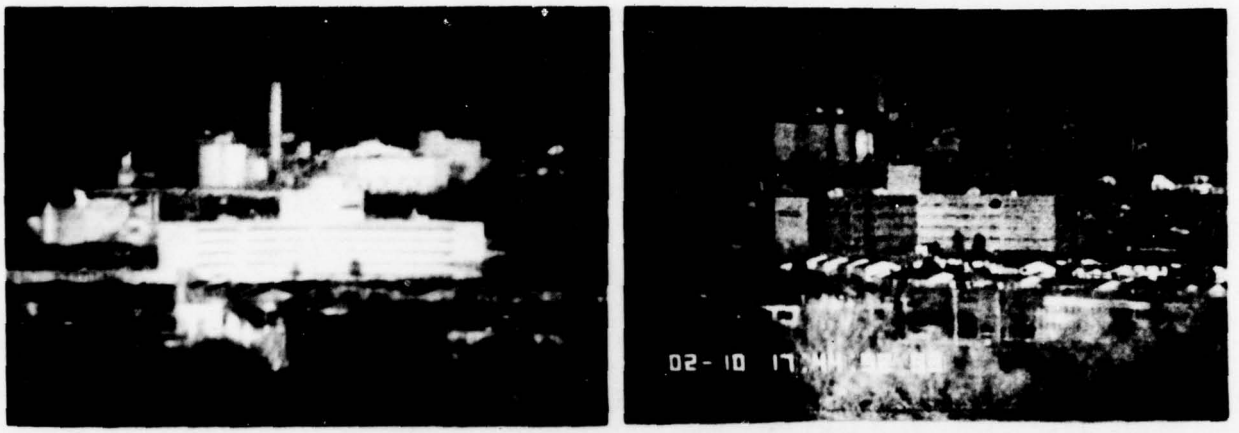

(a) Cool clear day, evening (Winter) (b)

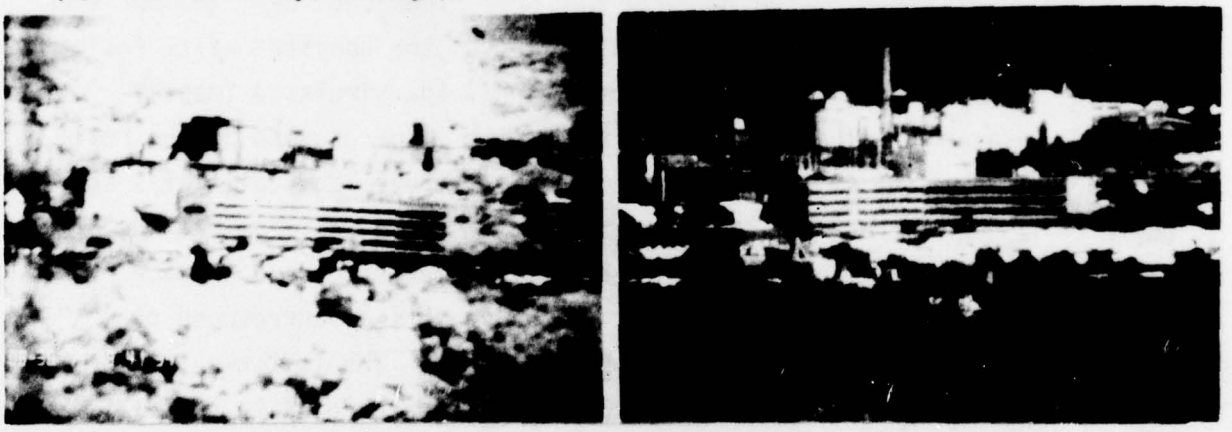

(c) Hot overcast day, early afternoon (Summer)

(e) Warm partially clouded day, noon (Fall) (f)

Figure 18. Images of the Actual Scene

TABLE 1. ENVIRONMENTAL CONDITIONS

Season	Day	Cloud	Temperature	Wind
Winter	7 February 1976	Clear	Cold	Windy
Summer	3 September 1976	Clear	Warm	Still
Fall	7 October 1976	Cloudy	Cool	Still

4.1 ACTUAL VS. SIMULATED IMAGERY

Figure 18 shows the imagery of the hospital scene taken by the actual LLLTV (18a, 18c, and 18e) and the FLIR (18b, 18d, and 18f) sensors. In the first photo taken by the LLLTV sensor on a clear cool day, the position of the sun is clearly indicated by the shades of the hospital walls facing towards the observer (Figure 18a). Notice that the simulated imagery for winter provides a good approximation of the image as seen by the real sensor. On the same day, in the FLIR imagery (Figure 18b), all walls are quite bright but of uniform shade. Again, the simulated image has the same characteristics (Figure 19c). Images in Figures 18c and 18d are shown for 2 PM on a hot overcast day. These conditions correspond to those of the simulated summer images (Figure 19d). The last two images are at noon on a partially clear warm day which corresponds to the conditions of the fall images (Figure 19c). Notice that the resolution of the real sensors far exceeds that of even level IIIB (which is about 50 ft).

4.2 SIMULATED FLIR IMAGERY

4.2.1 Seasonal Variation

Figure 19 shows three images of level IIIB at various times of the year. Environment conditions defined for the simulation of these images were the same as in Fairborn, Ohio at 10 AM, on 7 February, 2 September, and 7 October 1976, respectively.

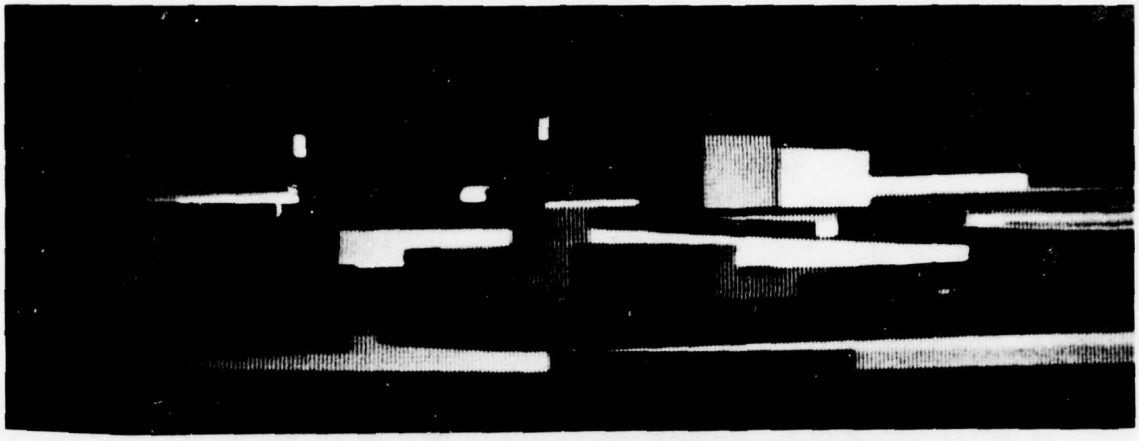

(a) Cool clear day (Winter)

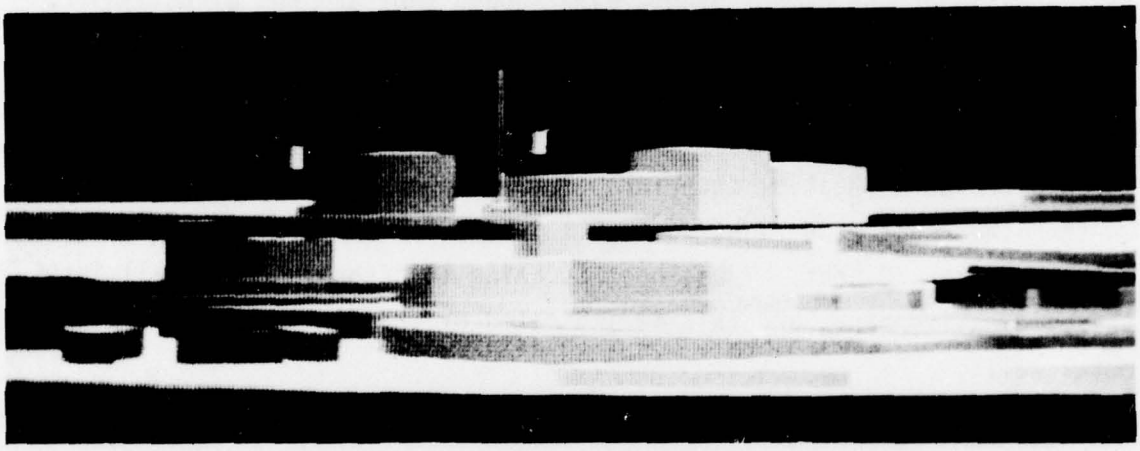

(b) Hot overcast day (Summer)

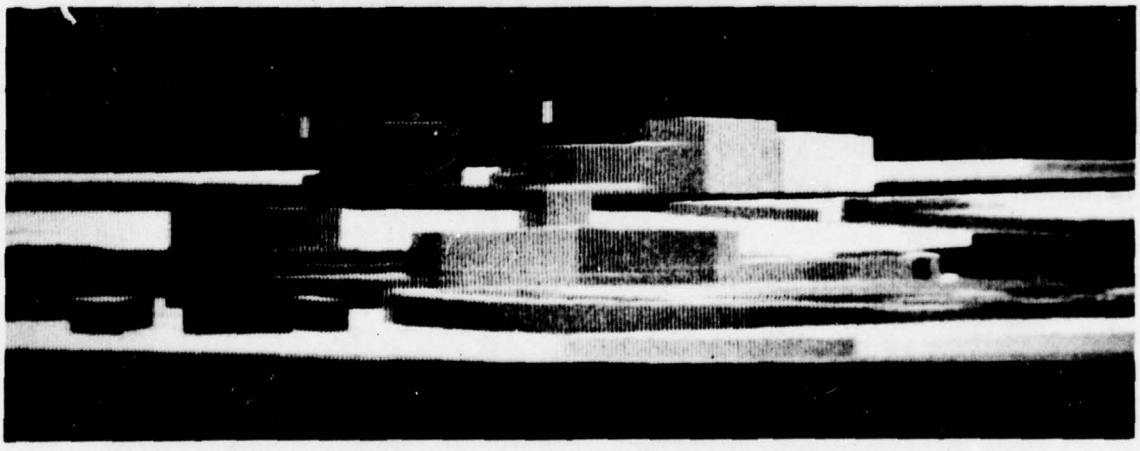

(c) Warm partially cloudy day (Fall)

Figure 19. Seasonal Variation for FLIR at Level IIIB

Winter - The winter day was a clear cool day with sky and air temperatures close to 40°F. The sun radiance was the most significant component of the heat loading. This resulted in a higher sensitivity of the walls to the position of the sun than on the other 2 days. As a consequence, walls facing in the direction of the sun are significantly warmer (indicated by a lighter shade) than are the walls facing away from the sun. For example, the south-facing wall of the hospital is quite warm, whereas the west-facing wall of the hospital, which is not irradiated directly by the sun, is still quite cold (Figure 19a). Also notice that the southwest-facing walls of the cement plant, even though they are not directly irradiated, display a noticeable temperature gradient. This illustrates the conductivity of the various materials. The left-most wall is concrete-block, and thus, acts as a fairly good insulator between the cold exterior and the warm (heated) interior. This accounts for its dark shade. On the other hand, the right-most wall is a metal structure and is a good conductor of heat. Thus, heat is being lost through this wall into the cold environment, and this is indicated by the light shade of this metal wall.

Summer - The environmental conditions for the typical summer day are hot and cloudy. The temperature at 10 AM was around 65°. Due to the cloud cover, the walls were not sensitive to the position of the sun as they were on a clear day in winter. All walls have fairly uniform shades since the air and the sky temperatures are the dominating heat load components. Sky radiance due to diffuse sun load is higher than in winter, and the roofs of the buildings have significantly higher temperature than walls. Thus, the temperature difference between the walls and roof is higher in summer than in winter. Moreover, the overall temperatures are higher than in either fall or winter, as indicated by the brighter image (Figure 19b).

Fall - The day for fall was a relatively clear, warm day. The temperature of the air was slightly lower than in summer. This causes the walls to be generally cooler (darker shade) than in the summer image. However, temperatures are still warmer than on the winter day (Figure 19c).

4.2.2 Diurnal Variation

Figure 20 gives the outlines of the major features in the scene together with positions of the sun at the various times of day. Figure 21 contains the simulated imagery of the scene at 7 AM, 10 AM, 1 PM, and 5 PM, respectively. Environment conditions at these times are the same as on 7 February 1976 in Fairborn, Ohio.

Early morning - At 7 AM, the sun is still below the horizon; thus the only thermal loading is due to the sky radiance and air temperature. All the walls have approximately the same shades since they are all uniformly loaded by the air temperature (Figure 21a). Notice that the roofs of the foreground buildings are significantly cooler (darker) than the corresponding walls. This is caused by the low temperature of the sky which forces the roofs to radiate heat.

Mid-morning - By 10 AM, the sun has risen above the horizon and is the major component of the heat load. This is reflected in the high contrast of the Figure 21b. Shades of the walls, especially those of the hospital, clearly indicate the position of the sun. South-facing walls of the hospital have significantly higher temperatures than the west-facing walls. This is because the sun is illuminating south-facing walls but not the west-facing walls (Figure 20). The roofs of the building in the foreground are at this time also illuminated by the sun, causing a reversal of relative temperatures of walls and roofs.

Afternoon - At 1 PM, the sun rises close to its highest position (apex) and subtends larger angles with the normals to the walls of the hospital (Figure 20). This results in brighter ground surfaces and

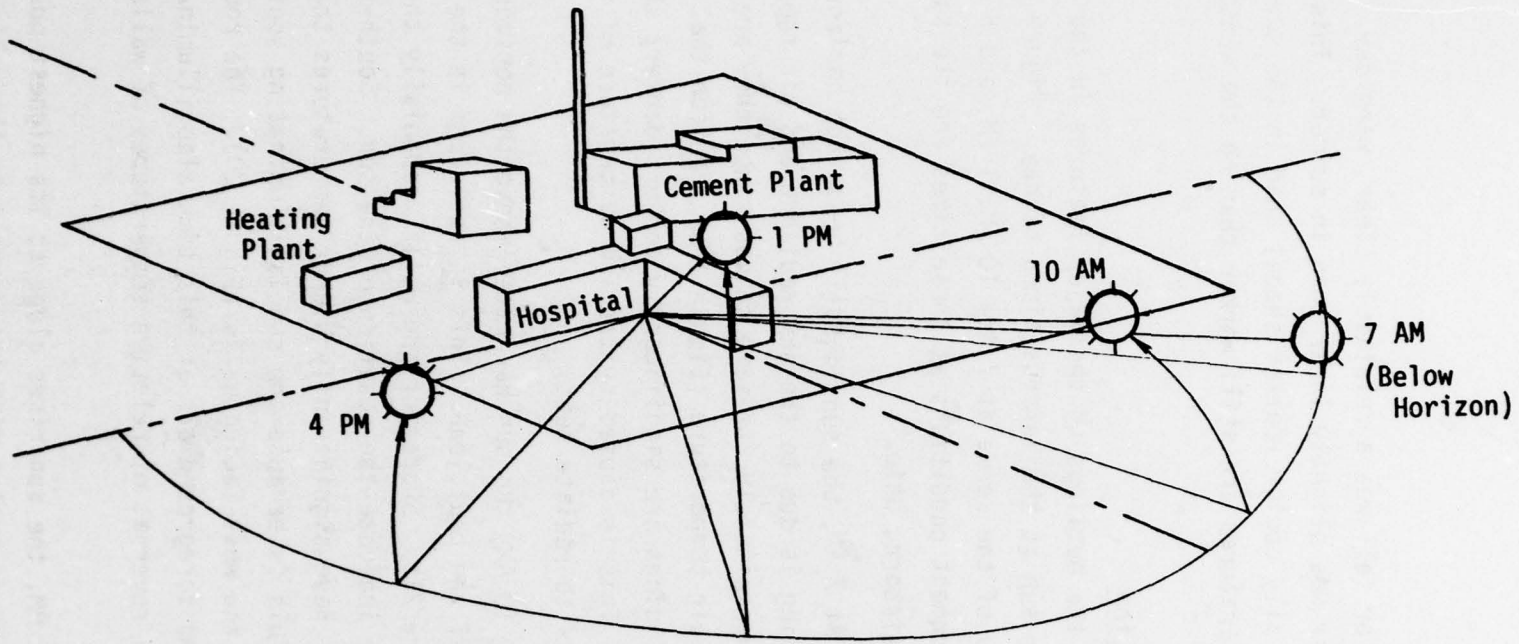

Figure 20. Outlines of the Major Features and Relative Sun Position

(a) 7 AM on a clear winter day

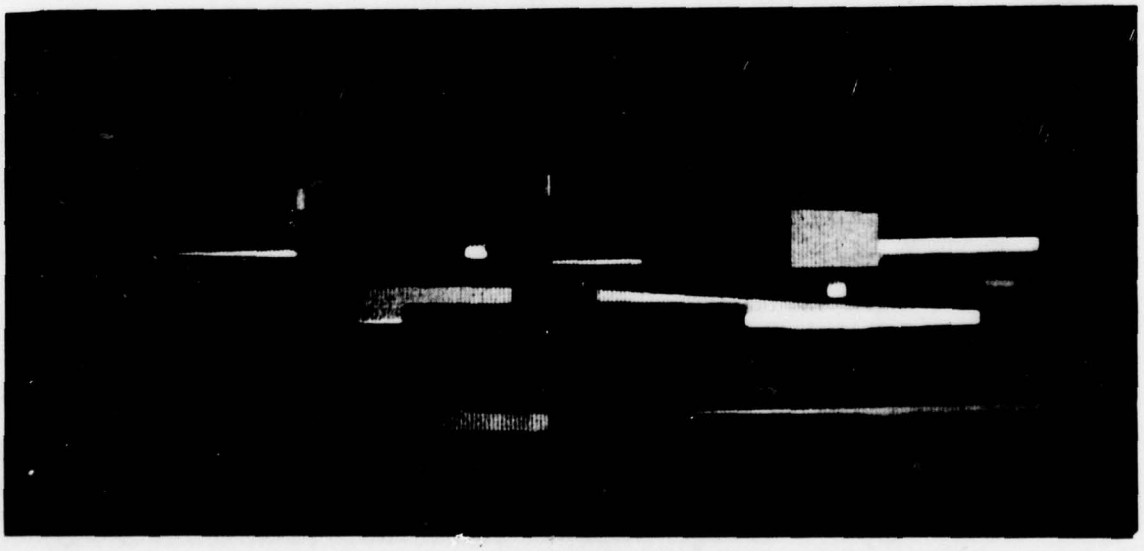

(b) 10 AM on a clear winter day

Figure 21. Diurnal Variation for FLIR at Level IIIB

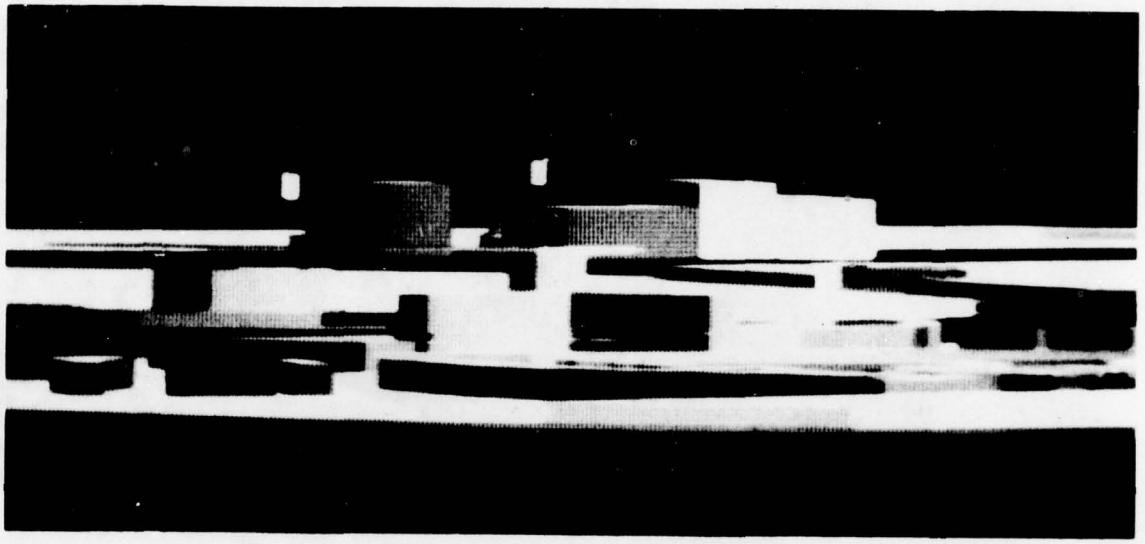

(c) 1 PM on a clear winter day

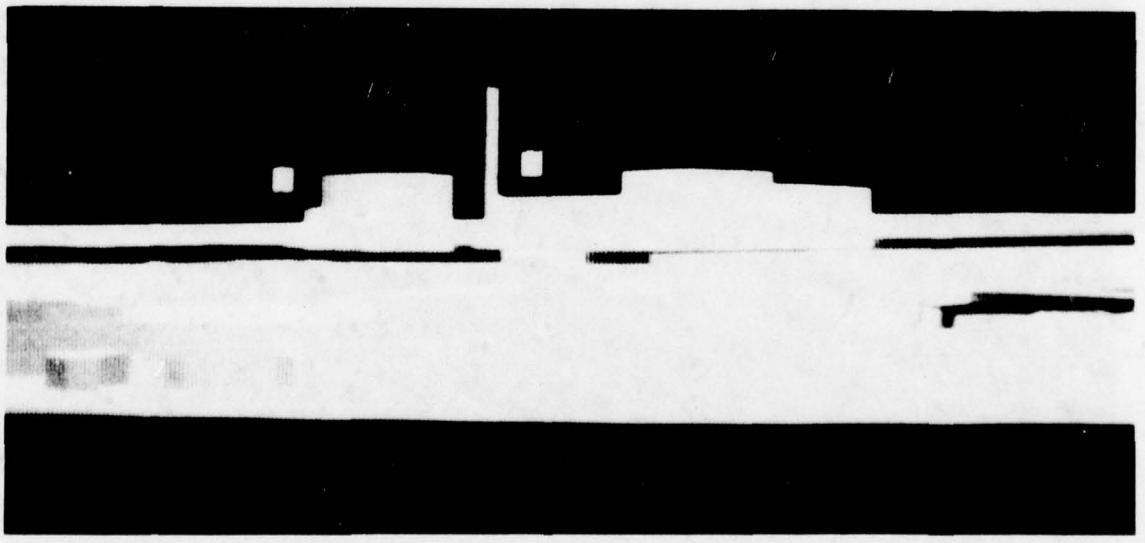

(d) 5 PM on a clear winter day

Figure 21. (Continued)

roofs, and insignificant change in the shades of the hospital walls as shown in Figure 21c. However, where at 10 AM the walls of the cement plant were not directly illuminated by the sun, they do face the sun by 1 PM. This accounts for the lighter shade of the cement plant walls when compared to the shades at 10 AM. Also, notice that the metal wall (right-most) is warmer then the concrete block wall (left-most). This is due to higher thermal conductivity of the metal when compared to the conductivity of the concrete.

Evening - By 5 PM, the thermal loadings due to the air temperature and the direct sun radiance are about equal. This produces the "washout" effect in Figure 21d, since the walls are not as sensitive to the position of the sun as they were in the middle of the day. Generally, all the shades are significantly lighter than during the morning hours, since they had time to warm up through the day and the thermal capacitance allows them to retain the heat into the early evening hours. Also, notice the shade reversal, especially on the heating plant walls. When compared to the shades through the rest of the day, walls facing south and west reverse their shades during early evening. This is caused by the passage of the sun throughout the day as indicated in Figure 20.

4.2.3 Levels IA and IIA

Images at the level IA have no large surfaces facing the observer; thus, during the diurnal variation, the sun position cannot be detected as easily as at the higher levels of detail. Only the overall change of the environment throughout the day can be traced in these images. Surfaces in the scene get progressively warmer as the sun rises and warms up the surrounding air as indicated by the gradual brightening of the images (Figure 22).

At level IIA, there are more individual features and both the position of the sun and the temperature of the environment are quite apparent (Figure 23). South-facing walls of all three major individual features (hospital, heating plant, and the cement plant) are warmer than the walls facing west, and the images become gradually lighter as the day progresses, just as they do in levels IA and IIIB.

4.3 SIMULATED LLLTV IMAGERY

Only two parameters are used in the visible model for the computation of the surface shades. The more significant of the two is the direct sun radiance. The other parameter is the diffuse sky radiance which is a magnitude smaller than the direct radiance. Surfaces in the model were thus very sensitive to the sun position, and all the images have in general higher contrast than the images in the thermal simulation.

4.3.1 Seasonal Variation

Figure 24 contains images at three seasons of the year. The first one is on 7 February which is a clear cold day with significant sun radiance; the second image is on a cloudy day on 3 September, and the third day is a relatively clear day on 7 October.

Winter - The most significant component of the illumination is the sun radiance; thus, the image has high contrast. Surfaces facing away from the direction of the sun are significantly darker than the surfaces facing toward the sun (Figure 24a). For example, the hospital walls facing south (Figure 20) are lighter than surfaces facing west.

Summer - On a cloudy day, Figure 24b, the scene is not as sensitive to the position of the sun as on a clear day. This is because the direct sun radiance is no longer significantly larger than the diffuse sky radiance. Illumination thus comes from both of these components, and the image contrast is reduced. Notice also that the overall

(a) 7 AM on a clear winter day

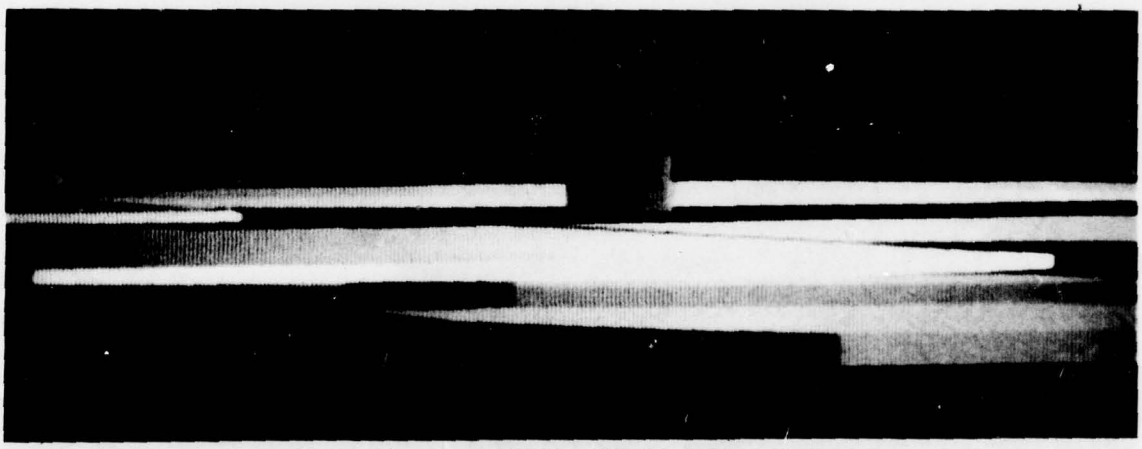

(b) 10 AM on a clear winter day

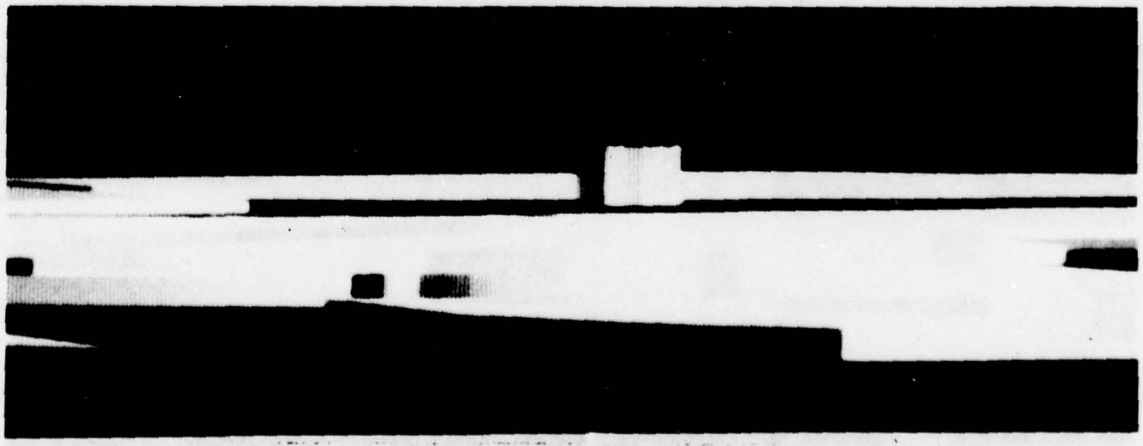

(c) 1 PM on a clear winter day

Figure 22. Diurnal Variation for FLIR at Level IA

(a) 7 AM on a clear winter day

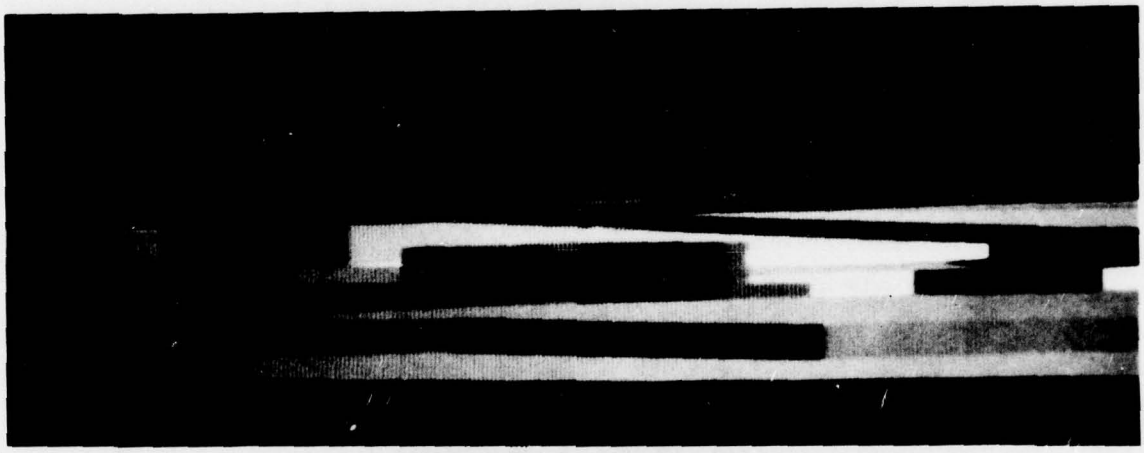

(b) 10 AM on a clear winter day

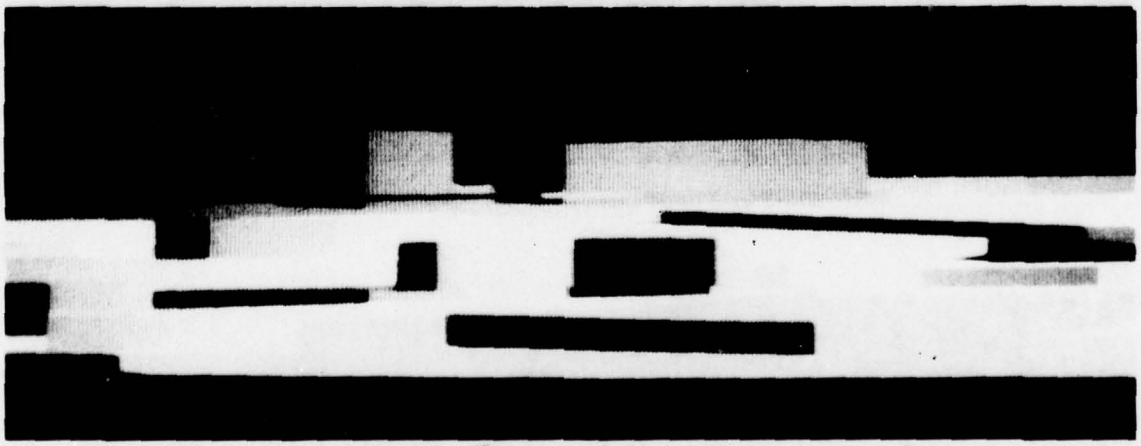

(c) 1 PM on a clear winter day

Figure 23. Diurnal Variation for FLIR at Level IIA

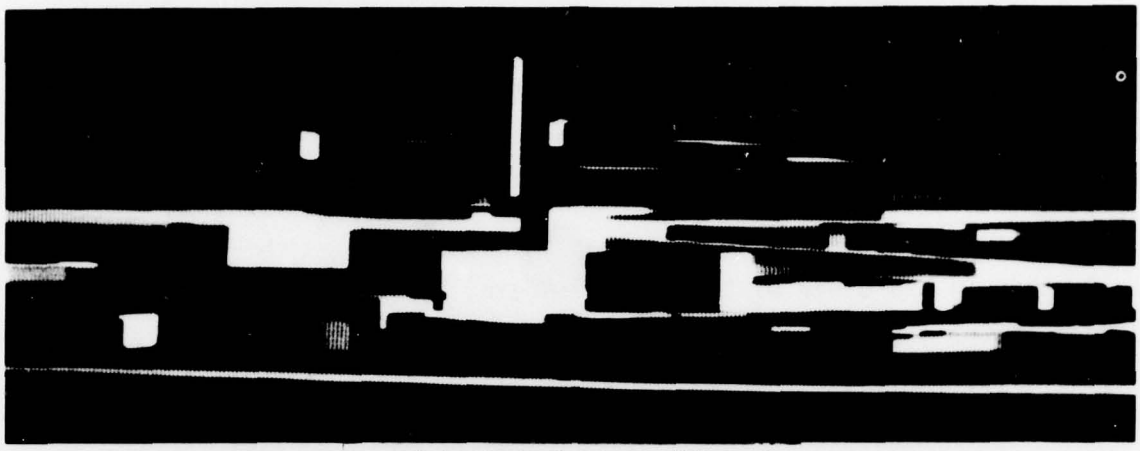

(a) Cool clear day (Winter)

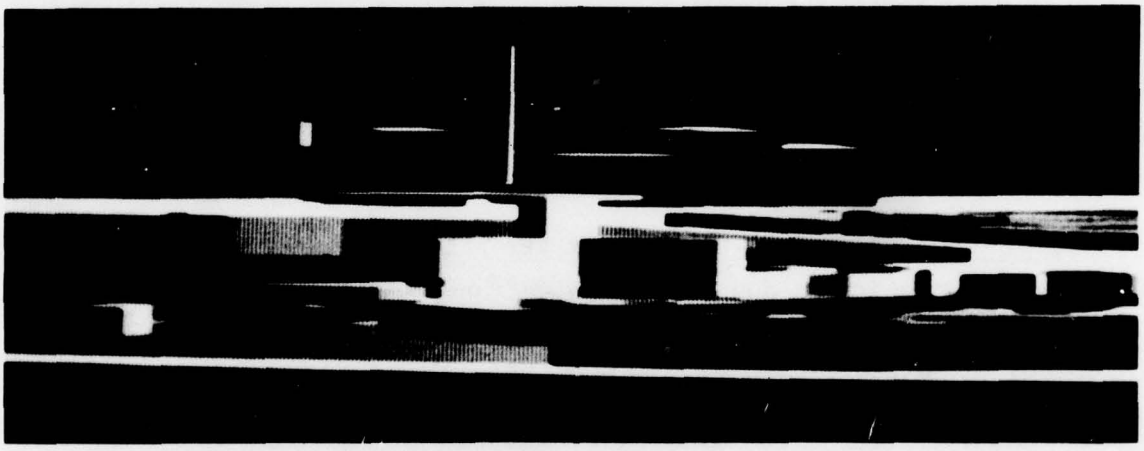

(b) Hot overcast day (Summer)

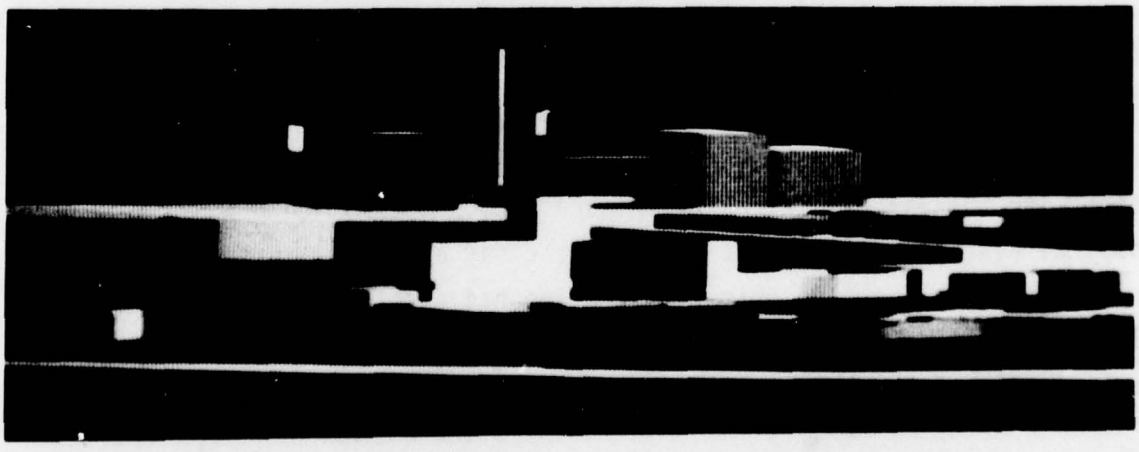

(c) Warm partially cloudy day (Fall)

Figure 24. Seasonal Variation for LLLTV at Level IIIB

illumination of the scene is reduced, and the image appears to be darker than on the clear day in winter.

Fall - Figure 24c is the image for a partially cloudy day, and thus the direct sun radiance is higher than in the summer cloudy image but lower than in the clear winter image. Again, as in the summer scene, clouds in the sky diffuse some of the direct sunlight and cause the sky to appear brighter than on the clear winter day. This accounts for the low contrast of the image.

4.3.2 Diurnal Variation

Images for 7 AM, 10 AM, 1 PM, and 4 PM, respectively, are shown in Figure 25 and are based on the level IIIB data base model. The sun position and intensity at all four times correspond to those on 7 February 1976 in Fairborn, Ohio.

Morning - At 7 AM, the sun has not yet risen above the horizon, and the only illumination is due to the sky radiance. All the surfaces have very similar shades causing the "washout" effect in Figure 25a. At 10 AM, the sun is still relatively low and to the east. The position of the sun is clearly indicated by the shades of the wall of the upper section of the hospital. Surfaces facing east are substantially brighter than the surfaces facing west (Figures 20 and 25b). However, the southwest walls of the cement plant face too far toward the west and thus are not illuminated.

Midday - At 1 PM, the sun is at its highest point and illuminates the scene with the maximum intensity (Figure 25c). South-facing walls of the hospital reach their lightest color of the day as do all surfaces parallel to the ground plane. At this time the sun has also advanced far enough to illuminate the southwest-facing walls of the cement plant and the west-facing walls of the hospital (Figure 20).

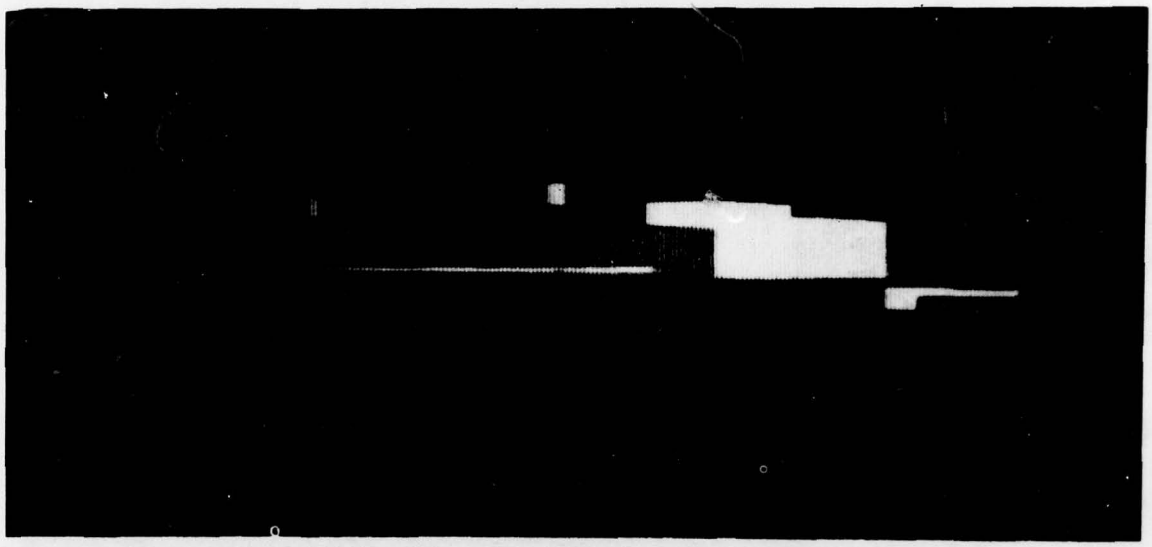

(a) 7 AM on a clear winter day

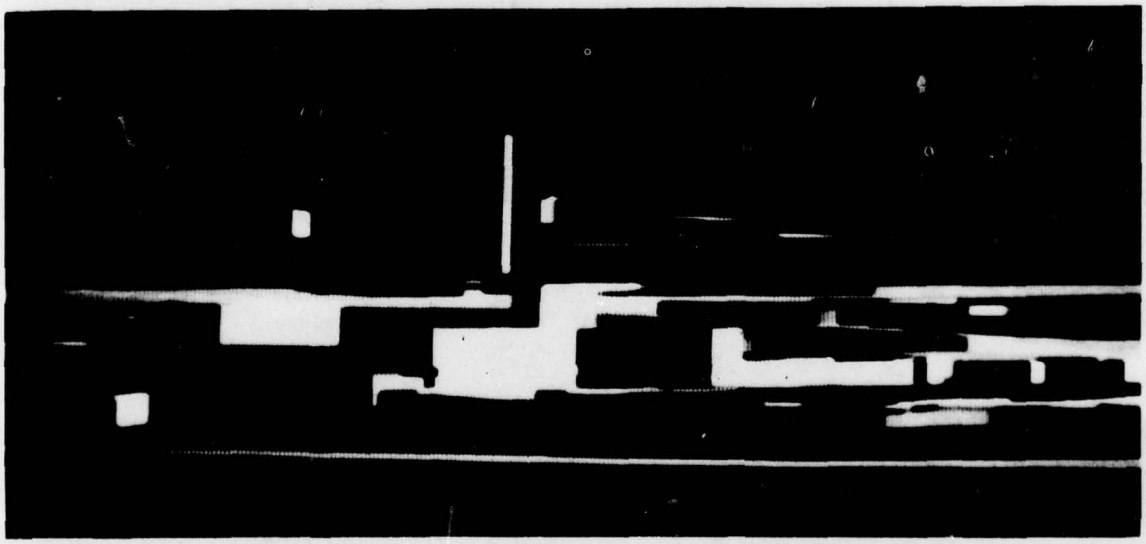

(b) 10 AM on a clear winter day

Figure 25. Diurnal Variation for LLLTV at Level IIIB

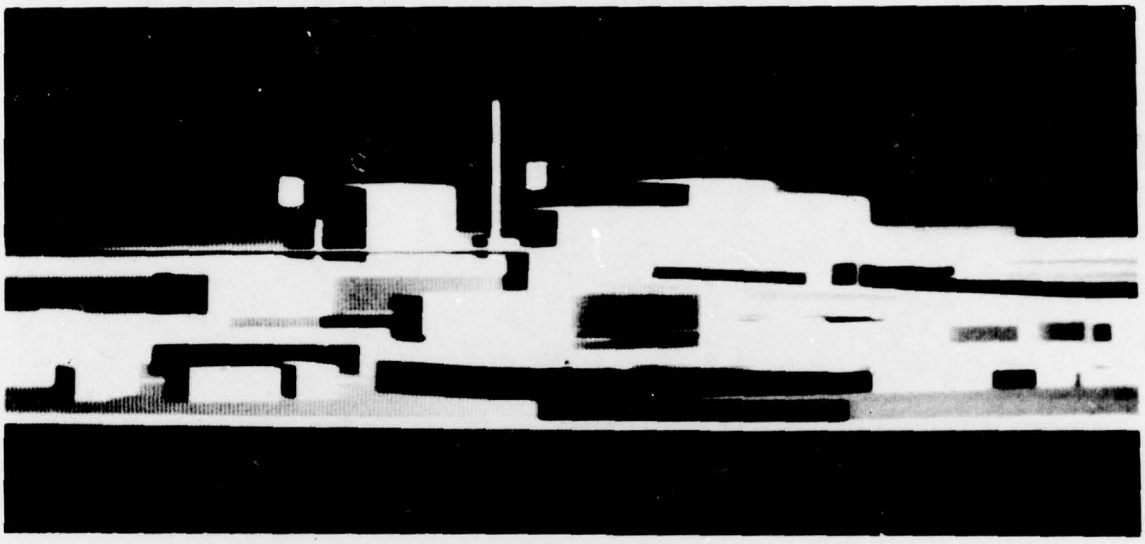

(c) 1 PM on a clear winter day

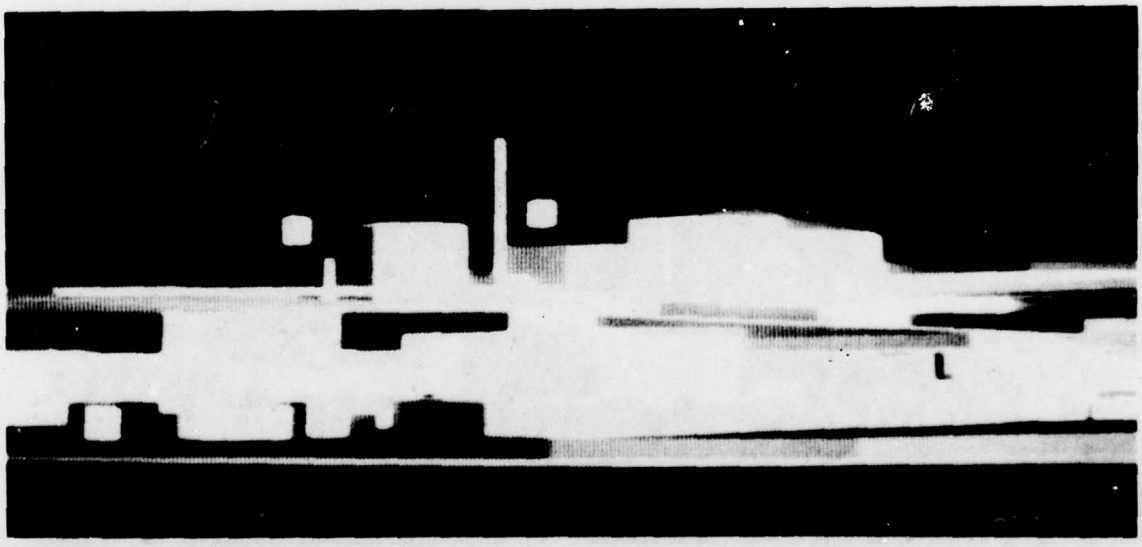

(d) 4 PM on a clear winter day

Figure 25. (Continued)

Evening - At 4 PM, the sun has moved to the west, and the south-west-facing walls of the cement plant are almost perpendicular to the direction of the sun. Thus, their shade reaches the brightest point of the day. The sun has advanced far enough to the west that the south-facing walls of the hospital are illuminated less than the walls facing west (Figure 25d). This accounts for the shade reversal of the hospital walls at 10 AM and 4 PM.

4.3.3 Levels IA and IIA

As was the case with the IR sensor, images of the level IA do not provide much information about the intensity or the position of the sun (Figure 26). Only the large surfaces parallel to the ground plane provide some indication of where the sun is. In particular, as the sun rises and the angle of incidence increases, surfaces parallel to the ground become lighter.

At level IIA, Figure 27, there are more individual features, similar to the IR images. However, the position of the sun cannot be determined from the individual surfaces.

(a) 7 AM on a clear winter day

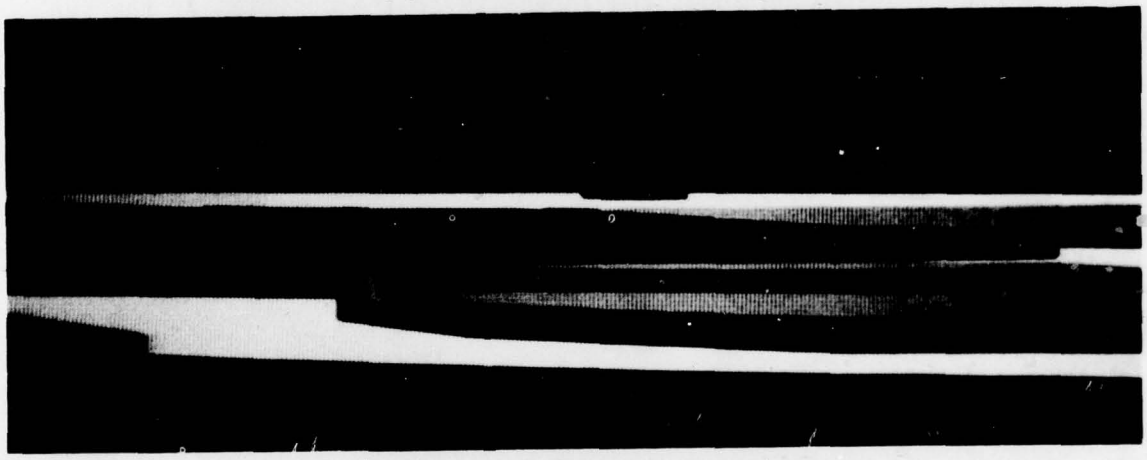

(b) 10 AM on a clear winter day

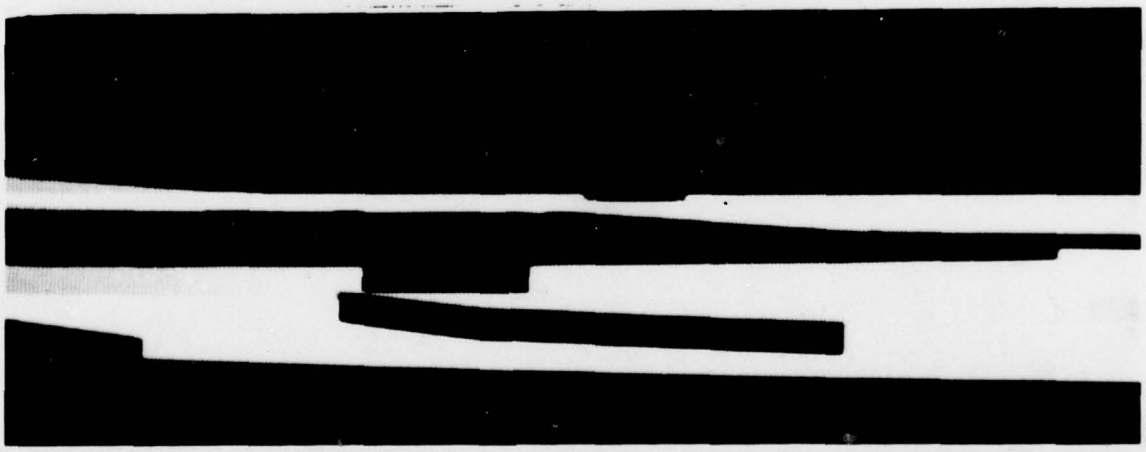

(c) 1 PM on a clear winter day

Figure 26. Diurnal Variation for LLLTV at Level IA

(a) 7 AM on a clear winter day

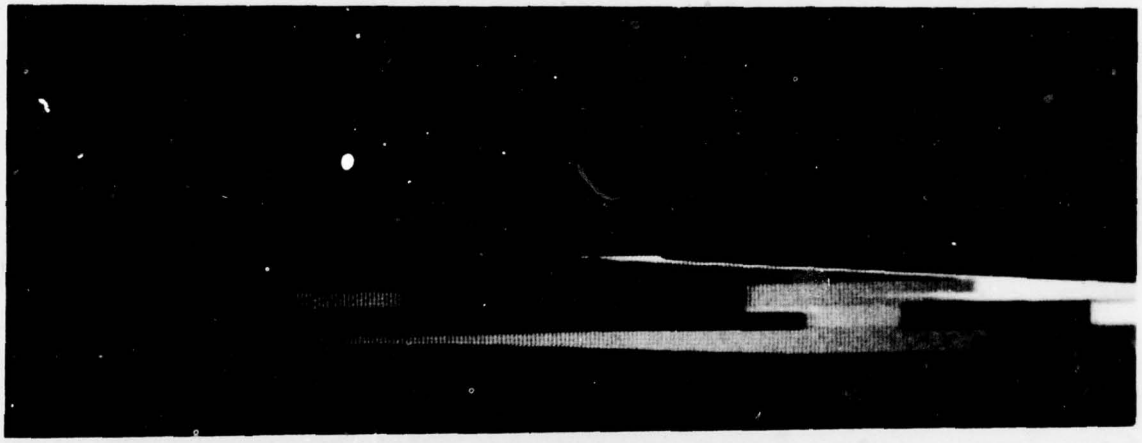

(b) 10 AM on a clear winter day

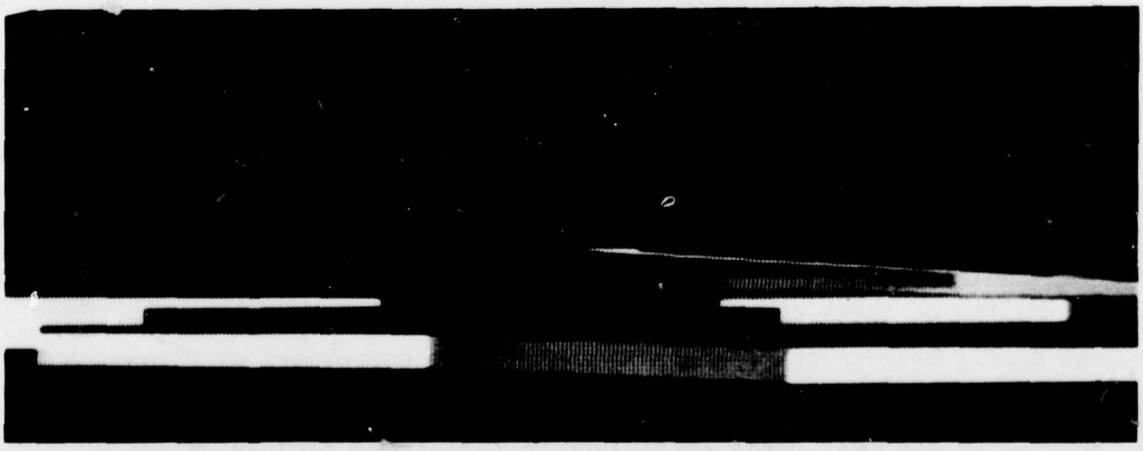

(c) 1 PM on a clear winter day

Figure 27. Diurnal Variation for LLLTV at Level IIA

V. IMPACT ON THE DMAAC DATA BASE

At this point, the major aspects of the project including the data base, tonal models, and imagery have been presented. The intent of this work was to evaluate data base descriptors and algorithms for LLLTV and FLIR simulation. In this section, the descriptors needed in LLLTV and FLIR simulations are presented, the descriptors available in the DMAAC data base are discussed, and a resolution of any discrepancy is attempted.

5.1 REQUIRED PARAMETERS

The data required to run a sensor simulation can be divided into three categories: scene data, environment data, and sensor data. The scene data consist of the shape and material description of the scene. The environment data consist of the electro-magnetic and thermal situation surrounding the scene at each instant. The sensor data consist of the performance behavior of a sensor in imaging the scene as illuminated by the environment. These data actually exist as parameters, i.e., position, material code, radiance, field of view, etc.

Parameters used in the simulation depend on the model and algorithms employed and are highly interrelated. As such, it is impossible to explicitly state a set of parameters that must be in a scene, environment, or sensor data base. Some parameters are derivable from other parameters, so that the choice of parameters used is sometimes arbitrary. With this in mind, minimal parameter sets and information derivable from data base parameters are useful ways of describing requirements on the data base.

Parameters are correlated with many aspects of a feature, and the utilization of these correlations is necessary in order to use the DMAAC data base. Surface and feature parameters are correlated with feature use, materials, location, size, age, and architecture. Architecture seems to be the best basis for inferring sensor-related parameters.

It is highly correlated to physical condition (i.e., accurate, highly descriptive, detailed, and compact). It is simply and accurately extracted from most available intelligence.

5.1.1 FLIR

The most difficult simulation is passive thermal. The scene signature has a thermal memory of up to several hours previous to the image; thus, the image is a result of numerous previous events. Figure 28 presents the significant categories of data and expected sources. FLIR simulation places heavy demands on the DMAAC data base and requires a full data description of the environment. The simulation requires as input a set of surfaces, material conditions of each surface, and the internal environment of each subset of surfaces forming a feature.

The general environment and internal feature environment provide boundary conditions for each surface for several simulated hours prior to the image time. The complete computation can be either executed each time surface shades are updated or stored in tables. Either way, the same demands are placed on the scene data base.

The work in Section III shows that surface cross section, absorptivity, orientation, and environment all play significant roles in forming a signature. These data are needed in any potential algorithm that generates accurate tones.

A high degree of simulation accuracy with respect to tonal rendition does not appear to be necessary for the training application. However, for passive infrared sensors, the intensities must be based upon parameters which include surface cross section, absorptivity, orientation and environment.

The number of thermal paths (conductive, convective, and radiative) and the time integration of their effects on a surface have a major impact on data base requirements. However, all paths, except to the sun, can be ignored (extreme simplification) provided the surface cross section, solar absorptivity, sensor band emissivity, orientation, and solar environment are known.

Categories of Data	Sources
Scene Data	
Shell	DMAAC-Like Scene Data Base
- set of surfaces	
Surface Materials	
- solar absorptivity	
- ground/sky absorptivity	
- sensor band absorptivity	
- surface cross section	
Feature Conditions	
- internal thermal environment	
Environment Data	
Sun	Simulated Mission Conditions (From Standard Type Environments or Actual Measurements)
- position	
- direct radiance	
- diffuse radiance	
Sky	
- thermal radiance	
Ground	
- thermal radiance	
Atmosphere	
- air temperature	
- wind vector	
- attenuation rate	
- precipitation	
Sensor Data	
Sensor Band	Sensor Performance Specifications
Field of View	
Scan Format	
Point Spread Function	
Response Curve	

Figure 28. Categories of Simulation Data and Their Sources for FLIR

5.1.2 LLLTV

The simulation of passive visible sensors is relatively easy. There are choices as to casting shadows and type of reflection (diffuse, diffuse plus specular, or general bidirectional reflection), but these choices have little impact on data base requirements. Figure 29 presents categories of data and expected sources. The demands are much less than for FLIR simulation.

The most significant requirements are on surface material parameters. Sensor band reflectivity and surface condition have important impact on surface radiance. In the visible band (actually a larger band from 0.2 to 3 microns), pigments and many other compounds have a significant and high, spectrally dependent effect on reflectivity.

5.2 AVAILABLE PARAMETERS IN THE DMAAC DATA BASE

The DMAAC data base serves as a scene data base meant to be complemented with environment and sensor data bases supplied elsewhere. It was basically designed to serve radar simulators.

The DMAAC digital data base provides a ground shell in the form of a terrain file and a planimetric (culture) file. The basic resolution is ten or more times lower than a typical E-O sensor, but the identification of discrete features, especially unique significant features, and the use of statistical measures, such as percent tree cover and number of structures per square mile, increase the shape data available to model a shell.

The manner in which the shell is represented as a set of feature ground perimeters produces shape distortions of walls, roofs, and small structures. The effects of shape distortions and omissions are noticeable, as seen in Section IV, but the shapes are generally interpretable in E-O imagery.

Surface material parameters must be derived from the material code and feature ID code of each feature. The correlation of surface material parameters with the given data is low. For example, roofs and walls are not distinguished, and surface condition (smooth or rough), surface reflectivity in the visible band, surface cross section, etc., are not well correlated with available data.

Categories of Data	Sources
Scene Data	
Shell	DMAAC-Like Scene Data Base
- set of surfaces	
Surface Materials	
- sensor band reflectivity	
- surface condition (i.e., flat, corrugated)	
Feature Conditions	
- internal lighting	
Environment Data	
Sun	Simulated Mission Conditions
- position	
- direct sensor band radiance	
- diffuse sensor band radiance	
Atmosphere	
- attenuation rate	
Sensor Data	
Sensor Band	Sensor Performance Specifications
Field of View	
Scan Format	
Point Spread Function	
Response Curve	

Figure 29. Categories of Simulation Data and Their Sources for LLLTV

Some feature conditions, such as internal environment, are correlated with the feature ID code so it can be extracted.

In summary, much scene data is available but only in forms correlated with the physical parameters of the scene and its features. Some important data, such as visible band reflectivity and other surface parameters, are not included in the DMAAC data base.

5.3 RESOLUTION BETWEEN NEEDED AND AVAILABLE DATA

The tonal model developed in this effort requires more data than are presently available in the DMAAC data base in order to perform acceptable tonal assignment. The cultural file of the DMAAC source data contains information which reflects the general architectural character of the represented features. Although the provided resolution is low compared to the capability of FLIR and LLLTV sensors, this file remains the best source of real-world data available for use in the development of large cultural data bases.

It is possible that this file could be expanded to provide more of the data necessary for sensor simulation. Such an expansion would include a more detailed description of the geometrical and material properties of a feature as well as visible band reflectivity, surface cross section characteristics, and other relevant parameters.

There is, of course, considerable latitude at this point and continued studies should identify additional demands which can be placed on the data base as opposed to those which of necessity must be imposed on simulation contractors.

VI. CONCLUSIONS AND RECOMMENDATIONS

In this program, a model of the thermal properties of materials based on theoretical thermo-electromagnetic models was derived. Also, a data base of the dense, cultural hospital scene was constructed according to the DMAAC specifications. In addition, a program to evaluate the tonal model and generate imagery of the scene was designed and implemented. The simulated imagery shows the complete diurnal and seasonal variation of the LLLTV and FLIR sensor imagery. A key program feature is that the LLLTV and FLIR imagery was generated for the three DMAAC levels: IA, IIA, and IIIB. Finally, an initial assessment was made of the impact on DMAAC to include in the data base the additional description of the scene which is necessary to generate the passive imagery. However, the recommendations of adding the required information have been of general nature and contain no specific data definition. This is because the data requirements of the existing model are rather large. Thus, it remains to be determined what lesser amount of information is required to generate the images for different user applications.

Thus, a sensitivity analysis should be performed to test the effect of the many input parameters on the resultant imagery. Then factors of low sensitivity can be made constant and removed from the model. Factors which have the same sensitivity can be grouped together. Also, some input parameters may have an effect on the imagery when they are present together and little or no effect when only one element is present. These trend analyses should greatly reduce the input data requirements.

Once the data requirements have been refined, the next step is to determine which data should be included in the data base and how they can be included. Only those factors that affect the DMAAC data base should be identified, since a number of model parameters are concerned with the description of the sensor or environment. A result of this study will be a specific set of data base descriptors and the corresponding requirements on the DMAAC data base.

The tonal modeling and its subsequent incorporation with the geometric data base into a computationally efficient routine provide a practical yet realistic method of computing the tonal properties of cultural scenes. However, the model needs to be augmented in order to calculate the tonal properties of common natural features. A study effort for this purpose would capitalize on the existing theoretical model, the finite difference equation solution, and the software implementation. The key effort is to model the thermal properties of natural features.

The work reported here was all directed toward generating images of the hospital scene from the AFHRL Seasonal Sensor Handbook. There are other scenes in the handbook which have merit from a tactical or training context. In fact, LLLTV and FLIR imagery could be generated for any of the 16 scenes contained in the AFHRL Seasonal Sensor Handbook. In addition, scenes from existing or intended data bases used for pilot training or scenes of a tactical interest for bomber/navigator training could also be used. Thus, the principles derived here could be applied to other scenes to generate their passive signatures.

REFERENCES

1. Neitman, R. and M. Kompar, AFHRL Seasonal Sensor Handbook, Mead Technology Laboratories.

2. Zimmerlin, T., Tonal Modeling, Technology Service Corporation, Report TSC-PD-A182-1, 3 December 1977.

☆U.S. GOVERNMENT PRINTING OFFICE: 1979- 671-056/110